Supplemental material: *Escherichia coli* maintains pH via the membrane potential

Guillaume Terradot, Ekaterina Krasnopeeva, Peter S. Swain, Teuta Pilizota

Supplementary text

Cell shape. To calculate a cell's surface area and volume, we assume that the cell is a spherocylinder with a length-to-width ratio of 3:1, determined from our microscopy images [1] and consistent with [2], and write:

$$S = \pi w l \tag{S1}$$

$$V = \pi \left(\frac{w}{2}\right)^2 \left(l - \frac{w}{3}\right) \tag{S2}$$

where l, w, and V are the length, width, and volume of the cell. We take the cell width as 1 μm because it deviates very little from this value across differgrowth conditions [3]. When calculating osmotic pressure, we assume that cellular volume stays constant and ignore cell wall mechanical properties for simplicity.

Describing the movement of ions. To describe the movement of ions across the plasma membrane, we use Eq. 5, which is

$$\frac{d[x]_i}{dt} = -\frac{V_e}{V} \cdot \frac{d[x]_e}{dt} = j_x + \sum_a \sigma_a j_a \tag{S3}$$

where V_e is extracellular volume assumed to be constant, j_x the flux of ions due to leakage and j_a is the flux generated by pumping reaction a with a stoichiometric coefficient of $\sigma_{x,a}$ (Table S1).
We assume that all transport and leakage reactions can be modeled with Eq. 8 in the main text. We, thus, assume that all transport reactions are reversible and that the corresponding flux can be decomposed into the rate of import into the cell and the rate of export. For a transporter this is j_a^+ and j_a^-:

$$j_a = j_a^+ - j_a^- = j_a^+ \left(1 - \frac{j_a^-}{j_a^+}\right) \tag{S4}$$

where $j_a^+ \geq 0$ and $j_a^- \geq 0$. Similar would hold true for leakage.
The Gibbs free energy of this reaction, ΔG_a (Table S1), can be written as [4, 5]

$$\Delta G_a \equiv \frac{RT}{F} \ln\left(\frac{j_a^-}{j_a^+}\right), \tag{S5}$$

measuring ΔG_a in volts, using the definition of ΔG_a and writing $\Delta G_0 = -\log(K_{\text{eq}})/RT$ with detailed balance implying that the equilibrium constant K_{eq} is the ratio of the forward to backward rate constants. Eq. S4 then becomes

$$j_a = j_a^+ \left(1 - e^{\frac{F}{RT}\Delta G_a}\right) \tag{S6}$$

where j_a^+ is a function determined by the specifics of the transport [6].

Leakage reactions. For the leakage flux of ion x, we again use Eq. 8 in the main text, where j^+ is given as:

$$j_x^+ = \frac{S}{V} P_x x_e f_b(\Delta\psi) \tag{S7}$$

where P_x the membrane's permeability to x, and the functional form of $f_b(\Delta\psi)$ changes with the choice of approximation [7].
To describe the flux of ions from leakage we choose the trapezoidal energy barrier approximation [7] for all ions, which gives f_b as

$$f_b(z_x\Delta\psi) = \frac{\frac{F}{RT} b z_x \Delta\psi \cdot \mathrm{e}^{-\frac{F}{RT} z_x \Delta\psi/2}}{\mathrm{e}^{b\frac{F}{RT} z_x \Delta\psi/2} - \mathrm{e}^{-b\frac{F}{RT} z_x \Delta\psi/2}}. \tag{S8}$$

Here b is the fractional width of the trapezoid, $0 \leq b \leq 1$, which specifies how the electrostatic potential varies within the membrane [7].

Finally, inserting Eq. S7 and Eq. S8 into the Eq. 8 in the main text we get:

$$j_x = \frac{S}{V} P_x [x]_e f_b(z_x\Delta\psi) \left(1 - \mathrm{e}^{\frac{F}{RT}\Delta G_x}\right) \tag{S9}$$

When $b = 0$, Eq. S9 is Erying's single barrier model:

$$j_x(b=0) = \frac{S}{V} P_x [x]_e e^{-\frac{F}{RT} z_x \Delta\psi/2} \left(1 - e^{\frac{F}{RT}\Delta G_x}\right) \tag{S10}$$

when $b = 1$, Eq. S9 is the Goldman–Hodgkin–Katz flux equation [7].

The dynamics of protons and the dissociation of water. In our model, protons are the only ions whose pumping is powered by the cell's metabolism. Their electrochemical potential then powers all antiporters, making their dynamics the most complex. Using Table S1, we have

$$\frac{d[\mathrm{H_3O^+}]_i}{dt} = \underbrace{j_{\mathrm{H^+}}}_{leakage} \underbrace{-10j_{\mathrm{R}} + 3.3j_{\mathrm{F1fo}} + 3j_{\mathrm{NhaB}} + 2j_{\mathrm{NhaA}} + j_{\mathrm{ClcA}}}_{pumping} + f_w[\mathrm{H_2O}]_i^2 - b_w[\mathrm{H_3O^+}]_i[\mathrm{OH^-}]_i \tag{S11}$$

where f_w and b_w are rate of association of $\mathrm{H_3O^+}$ and $\mathrm{OH\_}$ and dissociation rate of $\mathrm{H_2O}$, respectively.
Hydroxide ions, on the other hand only leak according to

$$\frac{d[\mathrm{OH^-}]_i}{dt} = \underbrace{j_{\mathrm{OH^-}}}_{leakage} + f_w[\mathrm{H_2O}]_i^2 - b_w[\mathrm{H_3O^+}]_i[\mathrm{OH^-}]_i \tag{S12}$$

In practice, we use Eq. S11 only at steady state and consequently assume that the hydroxide ions are also at steady state:

$$j_{\mathrm{OH^-}} + f_w[\mathrm{H_2O}]_i^2 - b_w[\mathrm{H_3O^+}]_i[\mathrm{OH^-}]_i = 0 \tag{S13}$$

so that the terms from the ionisation of water in Eq. S11 can be replaced:

$$\frac{d[\mathrm{H_3O^+}]_i}{dt} = j_{\mathrm{H^+}} - 10j_{\mathrm{R}} + 3.3j_{\mathrm{F1fo}} + 3j_{\mathrm{NhaB}} + 2j_{\mathrm{NhaA}} + j_{\mathrm{ClcA}} - j_{\mathrm{OH^-}} \tag{S14}$$

To compute f_w in Eq. S13, we assume that the rates f_w and b_w are the same intracellularly and extracellularly. If $[\mathrm{H_2O}]_e = 1000/18$ M and b_w, the rate of association of hydronium and hydroxide ions, is diffusion-limited, so that $b_w = 10^{10}$ $\mathrm{M^{-1}\ s^{-1}}$ [8], then $f_w = K_w b_w / [\mathrm{H_2O}]_e^2$ or approximately 3.2×10^{-8} $\mathrm{M^{-1}\ s^{-1}}$, assuming $K_w = 10^{-14}$ $\mathrm{M^2}$.

Including bacterial volume regulation when describing the ion movement. As mentioned in the main text, Eq. S3 is a form of the pump-leak equations developed to understand the role of ions on the volume regulation of excitable cells [9], usually under the assumption that osmotic pressure is negligible [9, 10]. More recently, this assumption was relaxed in excitable cells with the membrane tension described by Hooke's law [11]. Doing so in bacteria, however, is more complex. For example, *E. coli*'s cell wall exhibits stress stiffening [12], and already does so under osmotic pressure [12, 1]. Additionally, *E. coli* opens mechanosensitive channels under higher tensions and not only uses ATP and IMF-driven import of ions and non-ionic osmolytes, but also synthesises some of these uncharged molecules [13]. Because of this ability to use uncharged molecules to control osmotic pressure, *E. coli*'s volume regulation is less coupled to ion flows than that of excitable cells, and the bacterium can more easily achieve a stable volume. This behaviour also justifies our choice of keeping the cell volume, V, fixed in the pump-leak equations. Doing so might change the exact values of $\Delta\psi$ but will not change the relationships between PMF and $\Delta\psi$ we discuss in the main text.

Bounds on the PMF. To determine physiological limits on the PMF we refer to the literature and again take a minimal approach. We define the respiratory regime by the coupling of the redox reaction $\mathrm{R}^\star \rightleftharpoons \mathrm{R}$, where $\mathrm{R}^\star$ is typically NADH, to the export of protons:

$$\mathrm{R}^\star + \sigma_{H^+,R}\,\mathrm{H}_i^+ \rightleftharpoons \mathrm{R} + \sigma_{H^+,R}\,\mathrm{H}_e. \tag{S15}$$

with $\sigma_{H^+,R}$ being the stoichiometric coefficient determining the number of protons moved across the membrane for each $\mathrm{R}^\star$. Writing ΔG_{NADH} as the redox reaction's potential, then

$$\Delta G_R = \Delta G_{\mathrm{NADH}} - \sigma_{H^+,R}\,\Delta G_{H^+} < 0 \tag{S16}$$

if protons are to be exported. These protons are used by the $\mathrm{F_1F_o}$ ATP synthase to generate ATP [14]:

$$\mathrm{ADP} + \sigma_{\mathrm{H},F_1F_o}\,\mathrm{H}_e \rightleftharpoons \mathrm{ATP} + \sigma_{\mathrm{H},F_1F_o}\,\mathrm{H}_i, \tag{S17}$$

and for the flux of ATP to be positive, we require:

$$\Delta G_{F_1F_o} = \sigma_{H^+,F_1F_o}\,\Delta G_{H^+} - \Delta G_{\mathrm{ATP}} < 0. \tag{S18}$$

Together, Eq. S16 and Eq. S18 bound the magnitude of PMF in the respiratory regime:

$$\frac{\Delta G_{\mathrm{NADH}}}{\sigma_{H^+,R}} < \Delta G_{H^+} < \frac{\Delta G_{\mathrm{ATP}}}{\sigma_{H^+,F_1F_o}} \tag{S19}$$

To estimate these limits, we use $\Delta G_{\mathrm{ATP}} \simeq$ -560 mV for exponentially growing cells respiring on glucose [15] and $\sigma_{H^+,F_1F_o} = 3.3$ [16] (see also ***E. coli* energy budget** below). For ΔG_R, we use -2290 mV from the Gibbs free energy of the half-reactions [17] and with 10 protons moved per NADH oxidised [18]. We thus find that

$$-229\ \mathrm{mV} < \Delta G_{H^+} < -170\ \mathrm{mV}\ . \tag{S20}$$

The fermentative regime is coarse grained by representing it with $\mathrm{F_1F_o}$ hydrolysing ATP to export protons, which requires $\sigma_{H^+,F_1F_o}\,\Delta G_{H^+} > \Delta G_{\mathrm{ATP}}$ or

$$\Delta G_{H^+} > -170\ \mathrm{mV}\ . \tag{S21}$$

A caveat is that the free energy of ATP hydrolysis and the stoichiometric ratio σ_{H^+,F_1F_o} may change in different extracellular environments [19, 20], which would modify the value of the PMF that separates the respiratory and fermentative regimes. For example, in Fig. 3D in the main text, although we obtained data in the presence of oxygen, we estimate the PMF at which we observe pH_i recovery to be in the fermentative regime. Thus, the free energy and stoichiometric ratio of ATP hydrolysis or of NADH reduction could have changed at high pH_e. Alternatively, cells in Fig. 3D in the main text may have switched to fermentation in alkaline stress.

Extracellular environment. We start with a solution of water with a pH of 7. To change pH_e, we add either acid $[\mathrm{AH}]_0$ or base $[\mathrm{COH}]_0$. To change the concentration of extracellular salt, we add $[\mathrm{CA}]_0$. Assuming equilibrium, we use the known dissociation and associations constants, conservation of mass, and the charge neutrality of the solution to define fully the extracellular environment.

Water, hydroxide ions, and hydronium ions obey

$$2\mathrm{H_2O} \rightleftharpoons \mathrm{H_3O^+} + \mathrm{OH^-} \tag{S22}$$

and defining the equilibrium constant of this reaction as K_c, we have that

$$K_c = \frac{[\mathrm{H_30^+}]_e[\mathrm{OH^-}]_e}{[\mathrm{H_2O}]_e^2}. \tag{S23}$$

Taking logarithms and writing $K_w = K_c[\mathrm{H_2O}]_e^2$, which is sometimes called the ionic product of water, then

$$\mathrm{pK}_w = \mathrm{pH}_e + \mathrm{pOH}_e \tag{S24}$$

where we use the prefix p to denote $-\log_{10}$.

The acid dissociates

$$\mathrm{AH} + \mathrm{H_2O} \rightleftharpoons \mathrm{A^-} + \mathrm{H_3O^+} \tag{S25}$$

with an equilibrium dissociation constant of K_c

$$K_c = \frac{[\mathrm{H_30^+}]_e[\mathrm{A^-}]_e}{[\mathrm{H_2O}]_e[\mathrm{AH}]_e}. \tag{S26}$$

and so a $\mathrm{pKa} = -\log_{10}(K_c[\mathrm{H_2O}])$ of

$$\mathrm{pKa} = -\log_{10}\left(\frac{[\mathrm{A^-}]_e[\mathrm{H_3O^+}]_e}{[\mathrm{AH}]_e}\right). \tag{S27}$$

Similarly, the base dissociates too

$$\mathrm{COH} \rightleftharpoons \mathrm{C^+} + \mathrm{OH^-} \tag{S28}$$

with a pKb of

$$\mathrm{pKb} = -\log_{10}\left(\frac{[\mathrm{C^+}]_e[\mathrm{OH^-}]_e}{[\mathrm{COH}]_e}\right). \tag{S29}$$

From conservation of mass, and assuming that the salt fully dissociates once added to the external environment

$$\mathrm{CA} \longrightarrow \mathrm{A^-} + \mathrm{C^+} \tag{S30}$$

so that $[\mathrm{CA}]_e \approx 0$, we have

$$\begin{aligned}[\mathrm{COH}]_0 + [\mathrm{CA}]_0 &= [\mathrm{COH}]_e + [\mathrm{CA}]_e + [\mathrm{C^+}]_e \\ &\simeq [\mathrm{COH}]_e + [\mathrm{C^+}]_e \end{aligned} \tag{S31}$$

$$\begin{aligned}[\mathrm{AH}]_0 + [\mathrm{CA}]_0 &= [\mathrm{AH}]_e + [\mathrm{CA}]_e + [\mathrm{A^-}]_e \\ &\simeq [\mathrm{AH}]_e + [\mathrm{A^-}]_e. \end{aligned} \tag{S32}$$

Lastly, charge neutrality implies that

$$[\mathrm{H_3O^+}]_e - [\mathrm{OH^-}]_e + [\mathrm{C^+}]_e - [\mathrm{A^-}]_e = 0. \tag{S33}$$

Given pH_e, $[\mathrm{AH}]_0$, $[\mathrm{COH}]_0$ and $[\mathrm{CA}]_0$, we then use Eqs. S24 to S33 to find the remaining concentrations.
First, from Eq. S24,

$$[\mathrm{OH^-}]_e = 10^{\mathrm{pH}_e - \mathrm{pK}_w} \tag{S34}$$

and, using Eq. S29 and Eq. S34, Eq. S31 becomes

$$[\mathrm{COH}]_0 + [\mathrm{CA}]_0 = \left(1 + 10^{\mathrm{pKb} + \mathrm{pHe} - \mathrm{pK}_w}\right)[\mathrm{C^+}]_e \tag{S35}$$

and, using Eq. S27 and definition of pH_e, Eq. S32 becomes

$$[\mathrm{AH}]_0 + [\mathrm{CA}]_0 = \left(1 + 10^{\mathrm{pKa} - \mathrm{pHe}}\right)[\mathrm{A^-}]_e. \tag{S36}$$

Second, if pH_e is acidic, we do not add base so that $[\mathrm{COH}]_0 = 0$. Then, we can express $[C^+]_e$ from Eq. S35 and using Eq. S33 we get

$$[\mathrm{A^-}]_e = \frac{[\mathrm{CA}]_0}{1 + 10^{\mathrm{pKb} + \mathrm{pHe} - \mathrm{pK}_w}} + 10^{-\mathrm{pH}_e} - 10^{\mathrm{pH}_e - \mathrm{pK}_w}. \tag{S37}$$

Third, if pH_e is alkaline, we do not add acid so that $[\mathrm{AH}]_0 = 0$. Then, we can express $[A^-]_e$ from Eq. S36 and using Eq. S33 we get

$$[\mathrm{C^+}]_e = \frac{[\mathrm{CA}]_0}{1 + 10^{\mathrm{pKa} - \mathrm{pH}_e}} - 10^{-\mathrm{pH}_e} + 10^{\mathrm{pH}_e - \mathrm{pK}_w}. \tag{S38}$$

By assuming that the salt fully dissociates, we have therefore completely specified the extracellular environment by Eq. S34, Eq. S37, and Eq. S38 given only $[\mathrm{CA}]_0$ and pH_e.

Model reactions. Summary of all the model's reactions

Flux	Reaction	Free Energy Change	Refs. (for stoichiometries)
j_w	$2H_2O_i \rightleftharpoons H_3O_i^+ + OH_i^-$	NA	NA
j_{H^+}	$H_e^+ \rightleftharpoons H_i^+$	ΔG_{H^+}	NA
j_{OH^-}	$OH_e^- \rightleftharpoons OH_i^-$	ΔG_{OH^-}	NA
j_{C^+}	$C_e^+ \rightleftharpoons C_i^+$	ΔG_{C^+}	NA
j_{A^-}	$A_e^- \rightleftharpoons A_i^-$	ΔG_{A^-}	NA
j_R	$R^\star + 10\ H_i^+ \rightleftharpoons R + 10\ H_e^+$	$\Delta G_R = \Delta G_{NADH} - 10\Delta G_{H^+}$	[21]
j_{F1F_o}	$ATP + 3.3\ H_e^+ \rightleftharpoons ADP + 3.3\ H_i^+$	$\Delta G_{F1F_o} = \Delta G_{ATP} + 3.3\Delta G_{H^+}$	[16]
j_{NhaB}	$3\ H_e^+ + 2C_i^+ \rightleftharpoons 3\ H_i^+ + 2\ C_e^+$	$\Delta G_{NhaB} = 3\Delta G_{H^+} - 2\Delta G_{C^+}$	[22]
j_{NhaA}	$2\ H_e^+ + C_i^+ \rightleftharpoons 2\ H_i^+ + C_e^+$	$\Delta G_{NhaA} = 2\Delta G_{H^+} - \Delta G_{C^+}$	[23, 24]
j_{ClcA}	$H_e^+ + 2A_i^- \rightleftharpoons H_i^+ + 2\ A_e^-$	$\Delta G_{ClcA} = \Delta G_{H^+} - 2\Delta G_{A^-}$	[25]

Table S1. Summary of all the reactions we consider in the model.

A mathematical model of the membrane potential. To solve Eq. 2 in the main text, we first rewrite it as

$$\Delta\psi = \frac{FV}{SC_m}\left(z_Y[Y]_i + [H^+]_i - [OH^-]_i + [C^+]_i - [A^-]_i\right) \tag{S39}$$

where Y_i are the captive molecules with valency z_Y. Next we express $[C^+]_i$ and $[A^-]_i$ as a function of $[C^+]_e$ and $[A^+]_e$ using the definition of ΔG :

$$\Delta\psi = \frac{FV}{SC_m}\left(z_Y[Y]_i + [H^+]_i - [OH^-]_i + [C^+]_e \cdot e^{\frac{F}{RT}(\Delta G_{C^+} - \Delta\psi)} - [A^-]_e \cdot e^{\frac{F}{RT}(\Delta G_{A^-} + \Delta\psi)}\right). \tag{S40}$$

As discussed in the main text, we disregard the negligible contribution of $[H^+]_i$ and $[OH^-]_i$. Given our assumptions on *E. coli*'s shape, and taking into account its width changes very little from 1 µm [3], the surface to volume ratio is $\sim 4.25 \times 10^6$ m^{-1}, and using the previously reported $C_m \sim 6.5 \times 10^{-3}$ F m^{-2} [26], we find that $\frac{FV}{SC_m} \sim 3.5$ V per mM.

With the above assumptions, $\Delta\psi$ becomes

$$\Delta\psi = 3.5 \cdot \left(z_Y[Y]_i + [C^+]_e \cdot e^{\frac{F}{RT}(\Delta G_{C^+} - \Delta\psi)} - [A^-]_e \cdot e^{\frac{F}{RT}(\Delta G_{A^-} + \Delta\psi)}\right). \tag{S41}$$

Dividing Eq. S41 by $[\mathrm{Ion}]_e$, the total concentration of extracellular ions, we express Eq. S41 compactly as

$$\begin{aligned} 3.5 \cdot \frac{\Delta\psi}{[\mathrm{Ion}]_e} &= \alpha_Y + \alpha_{C^+} \cdot e^{\frac{F}{RT}(\Delta G_{C^+} - \Delta\psi)} - \alpha_{A^-} \cdot e^{\frac{F}{RT}(\Delta G_{A^-} + \Delta\psi)} \\ &= \alpha_Y + \sum_x z_x \alpha_x \cdot e^{\frac{F}{RT}(\Delta G_x - z_x\Delta\psi)} \end{aligned} \tag{S42}$$

where $\alpha_x = [x_e]/[\mathrm{Ion}]_e$ is the fraction of either cation or anion in the environment, with $\sum_x \alpha_x = 1$, and $\alpha_Y = z_Y[Y]_i/[\mathrm{Ion}]_e$ and with the total extracellular concentration of ions being

$$[\mathrm{Ion}]_e = [C^+]_e + [A^-]_e + [OH^-]_e + [H^+]_e. \tag{S43}$$

If pHe is acidic, then Eqs. S33, S34 and Eq. S37 imply that Eq. S43 becomes

$$\begin{aligned} [\mathrm{Ion}]_e &= 2\left([A^-]_e + [OH^-]_e\right) \\ &= 2\left(\frac{[CA]_0}{1 + 10^{\mathrm{pKb} + \mathrm{pH}_e - \mathrm{pK}_w}} + 10^{-\mathrm{pH}_e}\right). \end{aligned} \tag{S44}$$

If pH_e is alkaline, then the definition of pH, and Eqs. S33 and Eq. S38 imply that Eq. S43 becomes

$$
\begin{aligned}
[\mathrm{Ion}]_e &= 2\left([\mathrm{C}^+]_e + [\mathrm{H}^+]_e\right) \\
&= 2\left(\frac{[\mathrm{CA}]_0}{1+10^{\mathrm{pKa}-\mathrm{pH}_e}} + 10^{\mathrm{pH}_e-\mathrm{pK}_w}\right).
\end{aligned}
\tag{S45}
$$

For sufficiently large $[\mathrm{CA}]_0$, we approximately solve Eq. S42 for $\Delta\psi$ both by setting the left hand side of Eq. S42, which is small, to zero and by using $\alpha_{C^+} = \alpha_{A^-} \approx 1/2$.
This approximation:

$$
\alpha_Y = \frac{1}{2}\cdot\left(\mathrm{e}^{\frac{F}{RT}(\Delta G_{A_-}+\Delta\psi)} - \mathrm{e}^{\frac{F}{RT}(\Delta G_{C_+}-\Delta\psi)}\right)
\tag{S46}
$$

is robust for pH_e and pH_i in [4, 10] (Fig. S4) and we use it in Fig. 3.

$$
\Delta\psi \simeq \frac{FV}{SC_m}\left(z_Y[\mathrm{Y}]_i + [\mathrm{C}^+]_e\cdot\mathrm{e}^{-\frac{F}{RT}\Delta\psi} - [\mathrm{A}^-]_e\cdot\mathrm{e}^{\frac{F}{RT}\Delta\psi}\right)
\tag{S47}
$$

whose solution must hold both at and away from equilibrium. Therefore the membrane potential can never deviate substantially from the equilibrium potential if both the intracellular concentrations of protons and hydroxide ions remain negligible and there is no active transport of ions.

Antiporters with different stochiometries generate steady states with pH_i=7 for different ranges of PMF and pH_e. To understand why, we consider an NhaA-like antiporter when $z_Y[Y]_i = 0$ in Eq. 13 in the main text and pH_e is 5.5 (Fig. 1D in the main text – black line). The corresponding ΔpH is 1.5 and contributes -90 mV to the PMF. The antiporter exchanges cations ($x = C^+$) and $\Delta G_{A^-} = 0$. Consequently, $[A_i]$ passively follows the membrane potential with $[A_i] = [A_e]\exp(\frac{F\Delta\psi}{RT})$, increasing if $\Delta\psi$ becomes more positive, and vice versa.

For this NhaA-like antiporter, steady states become impossible for less negative PMFs (Fig. 1D in the main text), which, from Eq. 3 in the main text, require a more positive $\Delta\psi$ because ΔpH is fixed. A more positive $\Delta\psi$ increases $[A_i]$, and so, from Eq' 12 in the main text, can only be generated if $[C_i]$ increases. This increase in $[C_i]$ and the more positive $\Delta\psi$ raises ΔG_{C^+} via Eq. 1 in the main text until the upper bound of Eq. 11 in the main text is reached, and cations begin to leak out of, not into, the cell. If $z_Y[Y]_i$ is negative rather than zero, then for a given, sufficiently positive PMF, a given pH_e and a neutral pH_i, $[C_i]$ must be higher. These higher concentrations favour cations leaking from the cell and so lower the $\Delta\psi$ and hence the PMF at which the upper bound in Eq. 11 in the main text is reached (Fig. 1D top in the main text and S5).

Steady states also become impossible for sufficiently negative PMFs for an NhaA-like antiporter (Fig. 1D in the main text). Such PMFs require a more negative $\Delta\psi$ because ΔpH is fixed. This $\Delta\psi$ decreases $[A_i]$ and so can only be generated if $[C_i]$ decreases too. The decrease in $[C_i]$ and the more negative $\Delta\psi$ lowers ΔG_{C^+}. Exporting cations becomes harder until the lower bound of Eq. 8 in the main text is reached. The export of cations then stops, preventing a steady state. Although a more negative PMF does increase the free energy available to drive antiport, the corresponding decrease in $[C_i]$ dominates, and the overall free-energy change eventually becomes zero. If $z_Y[Y]_i$ is positive rather than zero, $[C_i]$ must be lower for a given PMF and pH_e. These lower concentrations make exporting cations harder, and so the point where the PMF is decreased sufficiently to stop export through the corresponding decrease in $[C_i]$ occurs at a higher PMF (Fig. 1D bottom in the main text and S3).

Energy budget of *E. coli*. To calculate the reference energy budget of *E. coli* (Fig. 4D), we used that *E. coli* growing at 0.89 h^{-1} on glucose consumes 19.8 mMh^{-1} of oxygen per gram of dry weight [27]. When growing at 1 h^{-1}, the dry weight of *E. coli* is 258 $\times$ 10 $^{-15}$ g per cell [28]. Assuming that the oxygen consumption and the mass per cell are comparable between the two experiments, we have that $19.8\times10^{-3}\times6\times10^{23}\times258\times10^{-15} = 3.08\times10^9$ O_2 consumed per cell per hour. With a stoichiometry of the respiratory chain of $\sigma_{\mathrm{H},R} = 10$ per 1/2 O_2 [21], this consumption rate corresponds to a 'budget' of 61.6×10^{10} protons per cell per hour.

Modelling the periplasm. We have considered a single barrier separating the cell's interior from its environment, but *E. coli* has an inner and an outer membrane [29]. The ionic pumps are all in the inner membrane [30, 31], and the outer membrane contains porins, which allow ions to move freely between the periplasm and the extracellular space [32, 33]. These ions should equilibrate so that the periplasmic and extracellular concentrations follow a Nernst equation. Setting Eq. 1 in the main text to zero, we obtain:

$$
[x]_p = [x]_e\cdot\mathrm{e}^{-\frac{z_xF}{RT}\Delta\psi_p}
\tag{S48}
$$

where $[x]_p$ is the periplasmic concentration of an ion x and $\Delta\psi_p$ is the equilibrium potential across the outer membrane, which will only be non-zero if the periplasm contains captive charged molecules.

From Eq. 1 and Eq. S48, we find:

$$\begin{aligned}[x]_i &= [x]_p \cdot \mathrm{e}^{\frac{z_x F}{RT}(\Delta G_x - z_x \Delta\psi)} \\ &= [x]_e \cdot \mathrm{e}^{\frac{z_x F}{RT}(\Delta G_x - z_x \Delta\psi_p - z_x \Delta\psi)}\end{aligned} \tag{S49}$$

Eq. S49 shows that $\Delta\psi_p$ offsets the extracellular concentrations 'felt' by at the inner membrane, so that the ΔpH between the cytoplasm and the periplasm differs from the ΔpH between the cytoplasm and the extracellular environment (Fig. S16). A $\Delta\psi_p$ of -30 mV [34] increases a cationic and decreases an anionic concentration by ~ 3.3 times.

Using Eq. S49, Eq. S41 becomes

$$\Delta\psi = \frac{FV}{SC_m}\left[z_Y[Y]_i + \sum_{x\in\text{small ion}} [x]_e \cdot \mathrm{e}^{\frac{F}{RT}(\Delta G_x - z_x\Delta\psi - z_x\Delta\psi_p)}\right]. \tag{S50}$$

Computational experiments.

Constants. All constants are specified in Table S2.

Name	Symbol	Units	Value	Ref.
Faraday constant	F	C/mole	96485	
Gas constant	R	J/mole/K	8.31	
Temperature	T	K	298	
Dissociation constant HCl	$\mathrm{pKa_{AH}}$	Dimensionless	-6.3	
Dissociation constant NaOH	$\mathrm{pKb_{COH}}$	Dimensionless	-0.56	
Dissociation constant H_2O	pKa_w	Dimensionless	14	
Association rate of H_3O^+ and OH^-	f_w	$\mathrm{M^{-1}s^{-1}}$	10^9	
Dissociation rate of H_2O	b_w	$\mathrm{M^{-1}s^{-1}}$	$3{\cdot}10^{-9}$	
Membrane capacitance	C_m	$\mathrm{F\ m^{-2}}$	6.5×10^{-3}	[26]
Cell width	w	m	1.07×10^{-6}	[2, 35]
Cell length	l	m	2.95×10^{-6}	[2, 35]
Gibbs free energy of NADH reduction	ΔG_{NADH}	V	-2.290	[17]
Gibbs free energy of ATP hydrolysis	ΔG_{ATP}	V	-0.560	[17]
Fractional width trapezoid	b	Dimensionless	1	Arbitrary
Proton permeability	$P_{\mathrm{H^+}}$	$\mathrm{m\ s^{-1}}$	10^{-4}	[7][1]
Hydroxide ion permeability	$P_{\mathrm{OH^-}}$	$\mathrm{m\ s^{-1}}$	10^{-4}	Arbitrary
Sodium permeability	$P_{\mathrm{C^+}}$	$\mathrm{m\ s^{-1}}$	5×10^{-10}	[36]
Chloride permeability	$P_{\mathrm{A^-}}$	$\mathrm{m\ s^{-1}}$	2×10^{-10}	[36]

Table S2. Constant parameters.

We obtained ΔG_{NADH} from eQuilibrator [17], which gives the Gibbs free energy of the half-reaction $\mathrm{NADH(aq) \rightleftharpoons NAD^+(aq) + 2}e^-$ as -64.1 kJ/mol and of the half-reaction $\mathrm{O_2(aq) + 4}e^- \rightleftharpoons \mathrm{2H_2O}$ as -314.5 kJ/mol at neutral pH and 100 mM ionic strength. Given that

$$\frac{1}{2}\mathrm{O_2 + NADH + H^+ \rightleftharpoons H_2O + NAD^+} \tag{S51}$$

then ΔG_{NADH}=$-64.1 - 314.5/2 = 221.3$ kJ/mole, which we convert to volts. Similarly, we use the standard Gibbs free energy for ATP hydrolysis of $\Delta G'^{\circ}_{\mathrm{ATP}} = -37.6$ kJ/mol [37] and assume that in *E. coli* [ATP] = 10 mM, [ADP] = 0.6 mM, and [Pi] = 20 mM [15]. Note that these values were reported for *E. coli* growing aerobically on glucose and are consistent in one case [38], and slightly higher in the other (2 mM) [39], obtained from single cell experiments also on *E. coli* grown aerobically on glucose. Thus, $\Delta G_{\mathrm{ATP}} = \Delta G'^{\circ}_{\mathrm{ATP}} + RT\ln([\mathrm{ATP}]/[\mathrm{ADP}]/[\mathrm{Pi}]) = -37600 + 8.31\times298\times\ln(0.01/0.02/0.0006) \approx -54$ kJ/mol, which we convert to volts (Table S2). From these values of ΔG_{NADH} and ΔG_{ATP}, we calculate the physiological values of the PMF for the respirative and fermentative regimes (Table S1).

Minimising the cost. Specifying the osmotic pressure, the PMF, intra- and extracellular pH, and the concentrations of all other extracellular ions, we define the cost of maintaining a given steady state as the flux of protons that are neither directly involved in generating ATP during respiratory growth nor are actively pumped by F_1F_o during fermentative growth:

$$\text{Cost} = j_{H^+} - j_{OH^-} + 3j_{\text{NhaB}} + 2j_{\text{NhaA}} + j_{\text{ClcA}} \tag{S52}$$

First, we emphasize that now all antiporters with equivalents in *E. coli*, NhaA, NhaB, ClcA, can pump simultaneously, where anions are pumped only by ClcA:

$$\frac{d[A^-]_i}{dt} = j_{A^-} - 2j_{\text{ClcA}} \tag{S53}$$

The steady-state equation for A^- is

$$j_{A^-} = 2j_{\text{ClcA}} \tag{S54}$$

or

$$j^+_{A^+}\left(1 - e^{\frac{F}{RT}\Delta G_{A^-}}\right) = 2j^+_{\text{ClcA}}\left(1 - e^{\frac{F}{RT}(\Delta G_{H^+} - 2\Delta G_{A^-})}\right) \tag{S55}$$

We know from Eq. 10 in the main text that $\Delta G_{H^+} < 0$, thus Eq. S54 requires both sides to be positive for a solution to exists, and hence

$$\frac{1}{2}\Delta G_{H^+} \leq \Delta G_{A^-} \leq 0 \tag{S56}$$

Similarly, we require

$$2\Delta G_{H^+} \leq \Delta G_{C^+} \leq 0 \tag{S57}$$

for there to be a steady-state solution for cations, because the steady-state equation for C^+ is

$$j_{C^+} = j_{\text{NhaA}} + 2j_{\text{NhaB}} \tag{S58}$$

or

$$j^+_{C^+}\left(1 - e^{\frac{F}{RT}\Delta G_{C^+}}\right) = j^+_{\text{NhaA}}\left(1 - e^{\frac{F}{RT}(2\Delta G_{H^+} - \Delta G_{C^+})}\right) + 2j^+_{\text{NhaB}}\left(1 - e^{\frac{F}{RT}(3\Delta G_{H^+} - 2\Delta G_{C^+})}\right) \tag{S59}$$

Again, we note that Eq. S58 requires Eq. S57 for a solution.

Second, from Eq. S13, $[H^+]_i$, and $[H_2O]_i = 55.56$ M, we calculate $[OH^-]_i$ at steady state, assuming that the leakage of hydroxide ions is described by Eq. S9. Then both j_{H^+} and j_{OH^-} in Eq. S52 are known. Specifically, we use here Erying's equation Eq. S10 to compute j_{H^+} and j_{OH^-} but could have used for instance GHK equation. Further, Eqs. S54 and S58 allow us to rewrite the cost in two ways:

$$\text{Cost} = j_{H^+} - j_{OH^-} + \frac{1}{2}j_{A^-} + \begin{cases} 2j_{C^+} - j_{\text{NhaB}} \\ \frac{3}{2}j_{C^+} + \frac{1}{2}j_{\text{NhaA}} \end{cases} \tag{S60}$$

either in terms of j_{NhaB} or j_{NhaA}.

Third, we combine the equation for the osmotic pressure

$$\frac{\Delta\Pi}{RT} = [Y]_i + [H^+]_i - [H^+]_e + [OH^-]_i - [OH^-]_e - [C^+]_e\left(1 - e^{\frac{F}{RT}(\Delta G_{C^+} - \Delta\psi)}\right) - [A^-]_e\left(1 - e^{\frac{F}{RT}(\Delta G_{A^-} + \Delta\psi)}\right) \tag{S61}$$

with the equation for the membrane potential

$$\frac{SC_m}{FV}\Delta\psi = z_Y[Y]_i + [H^+]_i - [OH^-]_i + [C^+]_e \cdot e^{\frac{F}{RT}(\Delta G_{C^+} - \Delta\psi)} - [A^-]_e \cdot e^{\frac{F}{RT}(\Delta G_{A^-} + \Delta\psi)} \tag{S62}$$

to express ΔG_{C^+} in terms of ΔG_{A^-} and z_Y, with all the other variables being specified.

We are now able to minimise the cost for these conditions. For negative membrane potential, and given Eq. S56, we simultaneously scan ΔG_{A^-} over this range and z_Y from $-10 \leq z_Y \leq 10$. For each value of ΔG_{A^-} and z_Y, we find ΔG_{C^+} from Eqs. S61 and S62. For these choices to be steady state, $[Y]_i$, found from Eq. S61 must not be negative, and Eq. S57 needs to hold.

For those values of ΔG_{A^-}, z_Y, and ΔG_{C^+} that satisfy these requirements and so allow a steady state, then j_{A^-} and j_{C^+} in Eq. S60 are known and computed according to Erying's equation Eq. S10. We need to consider only two further cases:

- If the calculated ΔG_{C^+} is such that $\frac{3}{2}\Delta G_{H^+} \leq \Delta G_{C^+} \leq 0$, then both j_{NhaA} and j_{NhaB} are positive from Eq. S59. The cost is minimised if j^+_{NhaA} is zero, using the lower branch of Eq. S60, and this minimal cost is given by Eq. S60 with $j_{\text{NhaA}} = 0$.
- If the calculated ΔG_{C^+} is such that $2\Delta G_{H^+} \leq \Delta G_{C^+} \leq \frac{3}{2}\Delta G_{H^+}$, then j_{NhaA} is again positive but j_{NhaB} is negative from Eq. S59. The cost is minimised if j^+_{NhaB} is zero, using the upper branch of Eq. S60, and this minimal cost is given by Eq. S60 with $j_{\text{NhaB}} = 0$.

For each scanned pair of ΔG_{A^-} and z_Y, we can therefore calculate the cost, and by comparing all pairs, we choose the ΔG_{A^-} and z_Y that give the minimal cost. For positive membrane potential we scan over ΔG_{C^+} and z_Y, in the exact same way as described above for ΔG_{A^-} and z_Y. In our scans, we explicitly include the case where no antiporters are needed: $\Delta G_{A^-} = \Delta G_{C^+} = 0$, which always minimises the cost if it allows a steady state. We find that when antiporters are used, the optimal z_Y is always at an extremum, either $z_Y = 10$ (when $\Delta\psi > 0$) or $z_Y = -10$ (when $\Delta\psi < 0$).

Approximating the optimal strategy Interestingly, we find numerically that for an arbitrary range of $z_Y \in [\min(z_Y), \max(z_Y)]$ and an osmotic pressure of 1 atm, the following strategy approximates well the optimal solution (Fig. S17):

1. If the desired membrane potential can be achieved by setting $\Delta G_{C^+} = \Delta G_{A^-} = 0$, the strategy is given by:

$$\begin{cases} z_Y & \text{given by Eq. S62} \\ j^+_{\text{ClcA}} & = 0 \\ j^+_{\text{NhaB}} & = 0 \\ j^+_{\text{NhaA}} & = 0 \\ \text{Cost} & = j_{H^+} - j_{OH^-} \end{cases} \tag{S63}$$

2. If the desired membrane potential is negative and cannot be achieved by setting $\Delta G_{C^+} = \Delta G_{A^-} = 0$, then set:

$$\begin{cases} z_Y & = \min(z_Y) \\ \Delta G_{A^-} & = 0 \text{ and } j^+_{\text{ClcA}} = 0 \end{cases} \tag{S64}$$

   and compute the corresponding electrochemical potential of cations required to achieve the desired $\Delta\psi$ given zero AMF. Depending on the value of this CMF, the solution is:

$$\text{if } \Delta G_{C^+} \in [3/2\Delta G_{H^+}, 0] \quad \text{then} \quad \begin{cases} j^+_{\text{NhaA}} & = 0 \\ j_{\text{NhaB}} & = 2j_{C^+} \\ \text{Cost} & = j_{H^+} - j_{OH^-} + \frac{3}{2} j_{C^+} \end{cases} \tag{S65}$$

$$\text{if } \Delta G_{C^+} \in [2\Delta G_{H^+}, 3/2\Delta G_{H^+}] \quad \text{then} \quad \begin{cases} j^+_{\text{NhaB}} & = 0 \\ j_{\text{NhaA}} & = j_{C^+} \\ \text{Cost} & = j_{H^+} - j_{OH^-} + 2j_{C^+} \end{cases} \tag{S66}$$

3. If the desired membrane potential is positive and cannot be achieved by by setting $\Delta G_{C^+} = \Delta G_{A^-} = 0$, then set:

$$\begin{cases} z_Y & = \max(z_Y) \\ j^+_{\text{NhaB}} = j^+_{\text{NhaA}} & = 0 \text{ and } \Delta G_{C^+} = 0 \\ j_{\text{ClcA}} & = 1/2 j_{A^-} \\ \text{Cost} & = j_{H^+} - j_{OH^-} + 1/2 j_{A^-} \end{cases} \tag{S67}$$

To compute leakage fluxes: j_{H^+}, j_{OH^-}, j_{C^+} and j_{A^-}, we use Erying's equation Eq. S10. Occasionally the membrane potential required to achieve a given pH_i, PMF, and osmotic pressure is simply not achievable for any state of the system. We then require the membrane potential to be the one with the minimal deviation of the resulting pH_i from the desired pH_i.

202 # Supplementary Figures

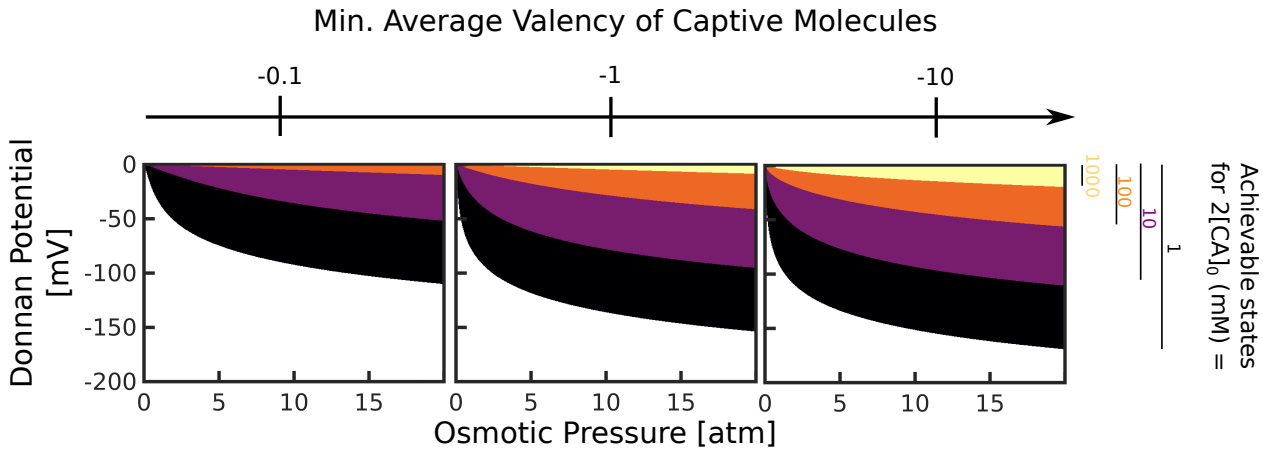

Fig. S1. Membrane potential can be maintained in thermodynamic equilibrium – Donnan potential – by captive charged molecules alone, but require low salinities of the medium, large average valencies of captive charges, and elevated osmotic pressures. We set $pH_i = pH_e = 7$, $\Delta G_{C+} = \Delta G_{A-} = 0$ and show the steady-state $\Delta\psi$ and $\Delta\Pi$ given a salinity $[CA]_0 \in \{0.5, 5, 50, 500\}$ mM and a minimal average valency of captive molecules. We note that the steady states achievable by $[CA]_0 = 0.5$ mM also includes those achievable for any value of $[CA]_0 > 0.5$ mM – all four coloured regions are achievable by setting $[CA]_0 = 0.5$ mM.

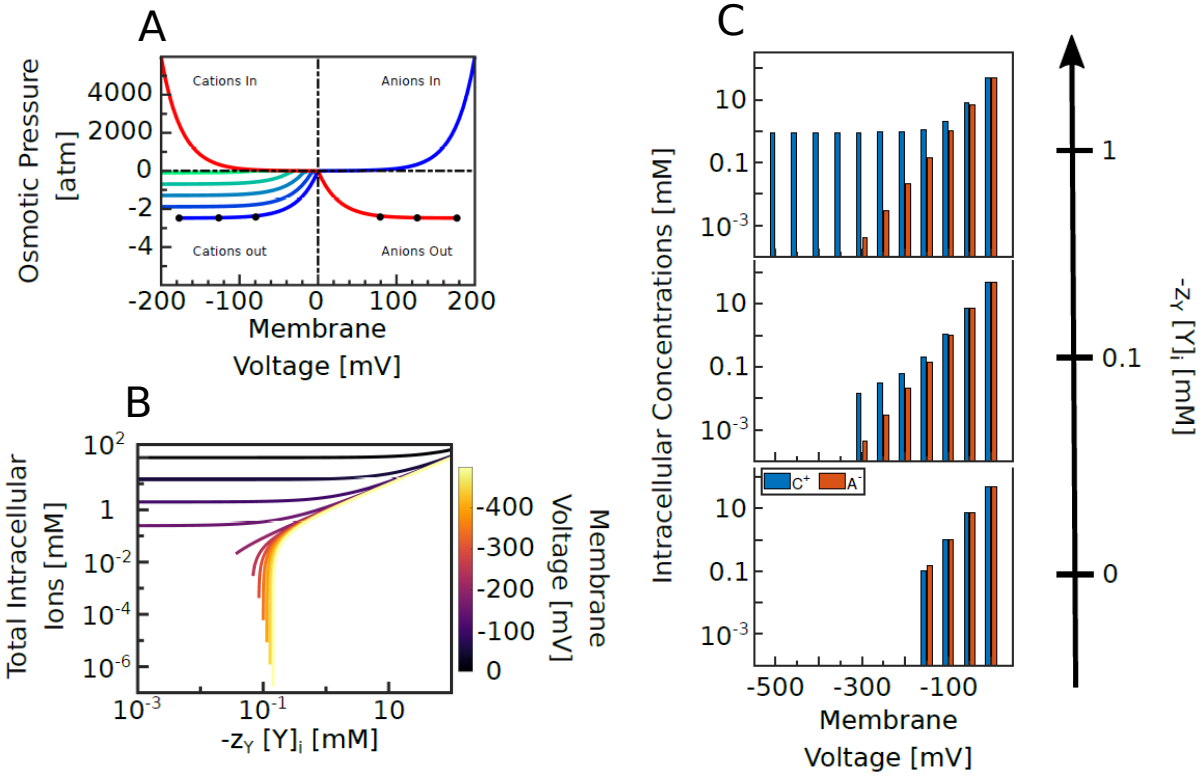

Fig. S2. Strategies for generating physiological $\Delta\psi$ and $\Delta\Pi$ (A) Osmotic pressure values (calculated only based on ion concentrations) plotted against $\Delta\psi$ when one cation (blue), or one anion (red), are pumped either in or out of the cell. To obtain the plotted $\Delta\psi$ values we set pH_i = 7. When only anions are pumped we set $\Delta G_{C+} = 0$ and vary ΔG_{A-} between ±500 mV, and similarly, when cations only are pumped we set $\Delta G_{A-} = 0$ and vary ΔG_{C+} between ±500 mV. $[Y]_i$ = 0 in all but the bottom left, where darkest blue indicates $[Y]_i$ =0 and lines from dark blue to light blue $[Y]_i$= 0, 12, 24, 36 and 48 % of the total extracellular ionic concentration ($[CA]_0$). Black dots on the dark blue line in the bottom left, and the red line in the bottom right indicate the minimum/maximum $\Delta\psi$ that can be reached for total extracellular ion concentrations of 1, 10 and 100 mM (the dot for 1 mM is the one closest to $\Delta\psi$ = 0). For all the other lines in the figure, $[CA]_0$=100 mM. Apart from the minimum/maximum value of $\Delta\psi$, changing the total extracellular ion concentration will not change $\Delta\psi$ behaviour. (B) $\Delta\psi$ (for cations pumped out) is composed of the contribution from the captive charges (x axis, only negative $z_Y[Y]_i$ are considered and the absolute value is plotted) and intracellular ions contribution (y axis). We set pH_e = pH_i = 7; $[CA]_0$ = 100 mM. Cells that harbour small amounts of $z_Y[Y]_i$ become increasingly depleted of small ions as they become more depolarised (the absolute value of $\Delta\psi$ increases). Since $\Delta\psi$ is maintained by pumping cations out, it becomes impossible to depolarize the cell further when $[C]_i \to 0$. (C) Intracellular ionic composition at different $\Delta\psi$ and for three values of $z_Y[Y]_i$. Pumping cations out results in $[A]_i$ > $[C]_i$ when $z_Y[Y]_i$ = 0 and $[C]_i$ > $[A]_i$ when $z_Y[Y]_i$ < -0.1 mM.

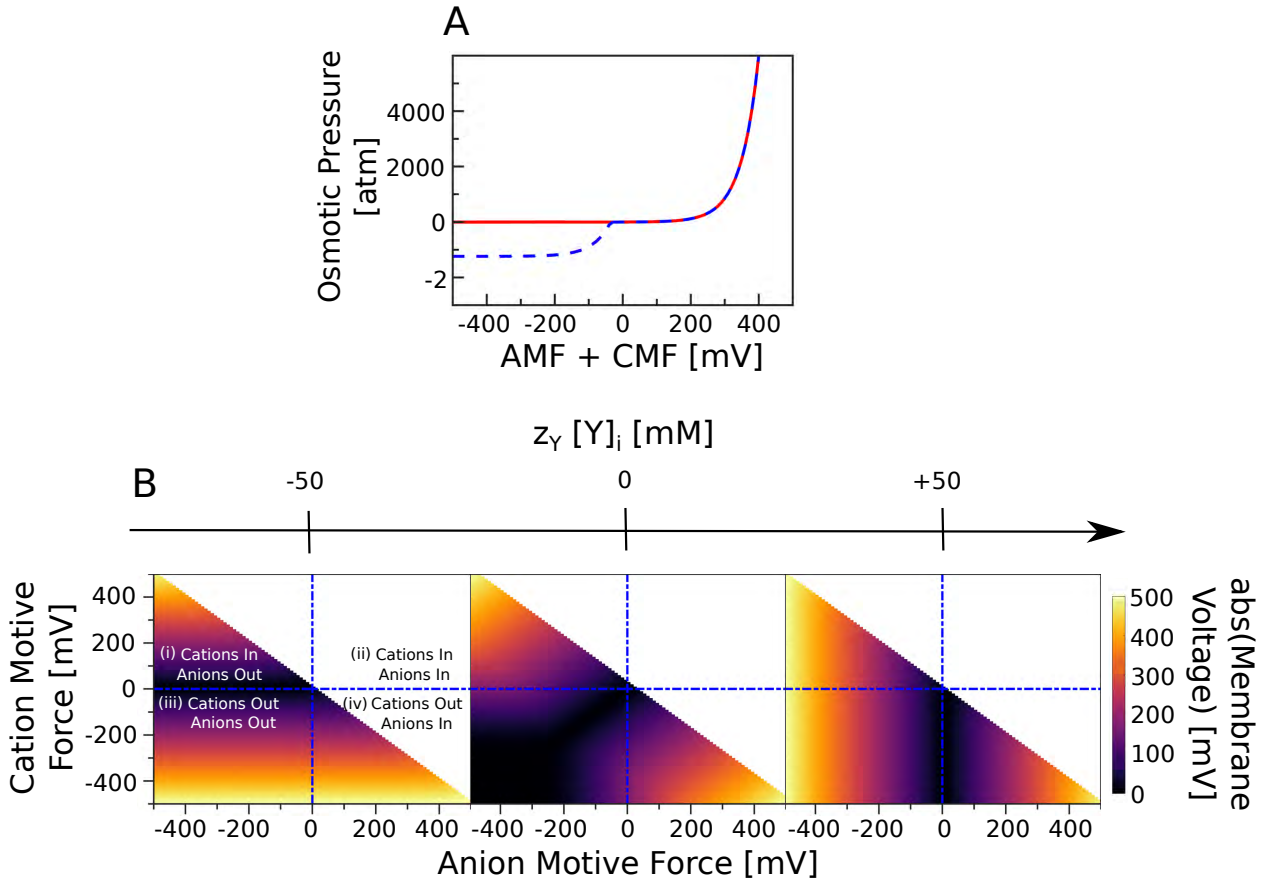

Fig. S3. Membrane voltage and osmotic pressure generated when both small cations and anions are pumped. We keep $[CA]_0$ = 50 mM, pH_i = pH_e = 7. (A) Relationship between osmotic pressure and AMF + CMF. Red and blue are for $z_Y[Y]_i$ respectively 0 and ±50 mM. Keeping the osmotic pressure in check translates to $\Delta G_{C+} + \Delta G_{A-} \leq 0$. The osmotic pressure is only a function of $z_Y[Y]_i$ and the sum of the ionic motive forces, irrespective of their relative values. (B) Absolute value of $\Delta\psi$ (colour map) is plotted for different CMF and AMF values; it is positive north-west and negative south-east. Only simulations resulting in $\Pi < 3$ atm are shown. $\Delta\psi$ is not sensitive to the AMF when $z_Y[Y]_i$ = -50 mM. Similarly, $\Delta\psi$ is insensitive to CMF when $z_Y[Y]_i$ = 50 mM.

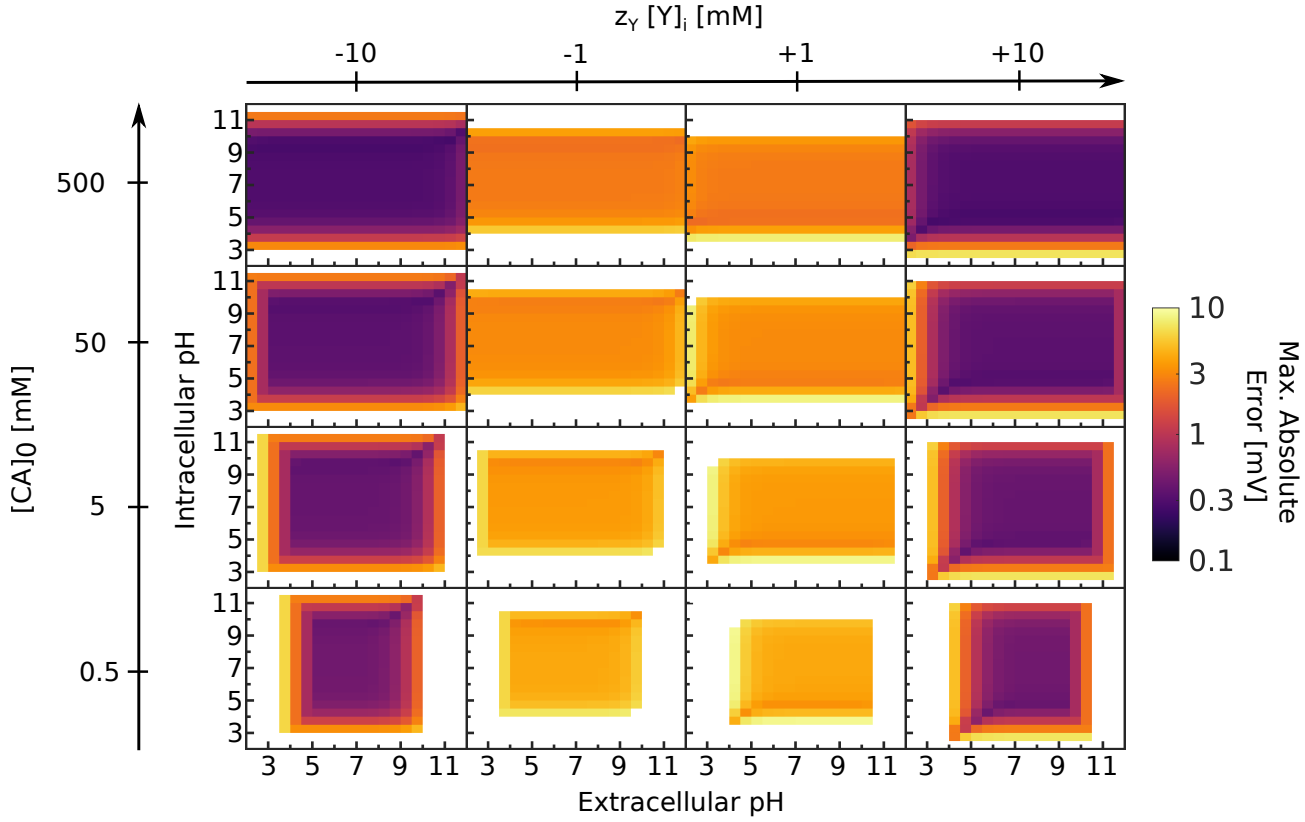

Fig. S4. Approximating the membrane potential gives low relative errors. We obtained $\Delta\psi$ in Fig. 1D by solving Eq. S41 for a fixed value of $[CA]_0$=50 mM. Here we plot the maximal absolute error in membrane potential if we assume that $[CA]_0$ is large and pH_e=7 and calculate $\Delta\psi$ using Eq. S46 instead. For a given $z_Y[Y]_i$, $[CA]_0$, pH_e and pH_i, we find the error for ΔG_{C_+} and ΔG_{A_-} varying over an 11×11 grid of equally spaced values within [-500,+500] mV, but show the maximal absolute error. The white regions correspond to maximum errors greater than 10 mV. For $z_Y[Y]_i = 0$ (not shown), the approximation always gives an absolute error greater than 10 mV.

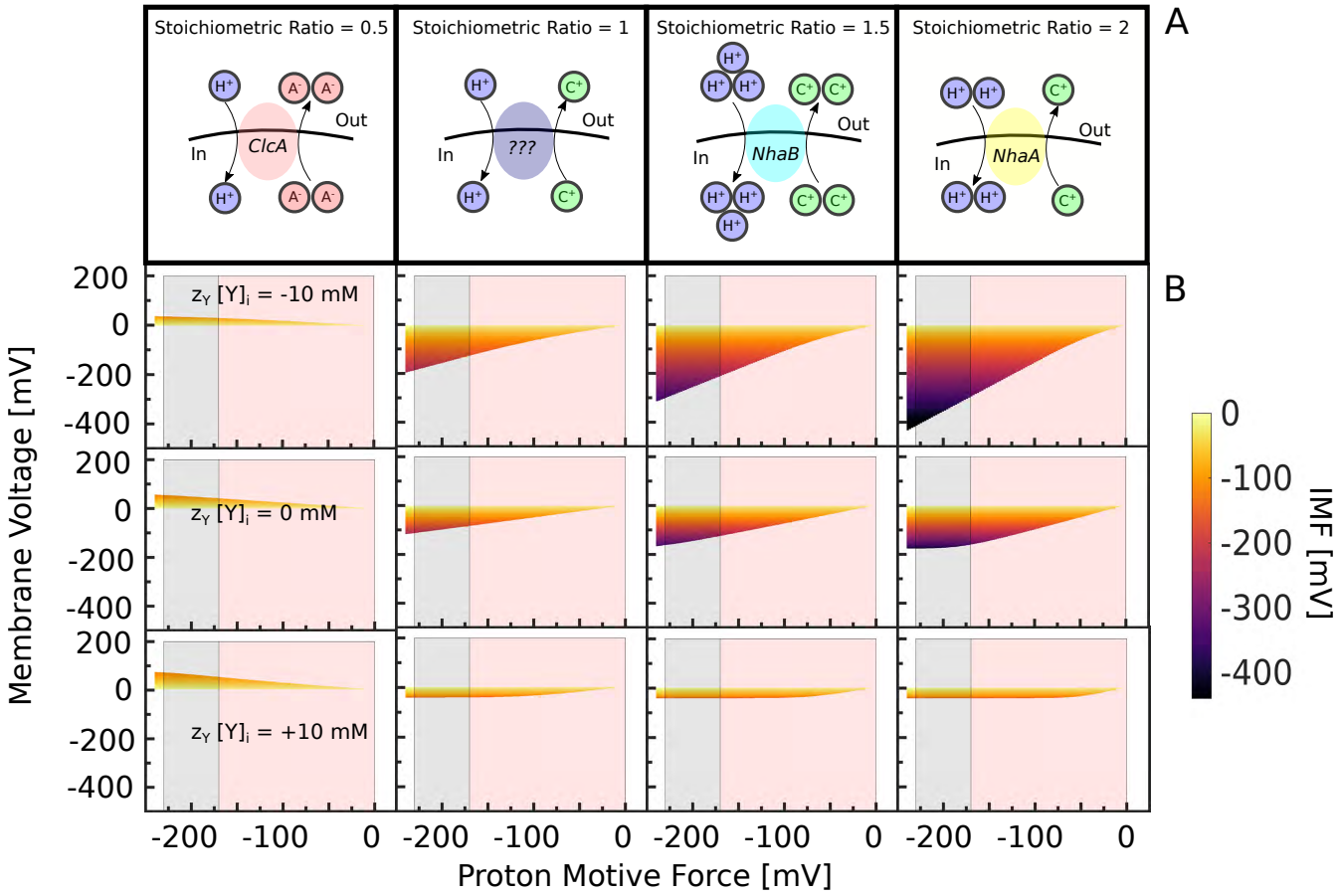

Fig. S5. The steady-state membrane potential required to maintain a neutral pH$_i$ for a given PMF. (A) Cartoon representations of the antiporters we study. (B) We set $[\mathrm{CA}]_0 = 100$ and pH$_i$ = 7 and show the range of membrane potential (y-axis) that can be maintained at steady state for each PMF (x-axis), as well as the corresponding IMF (colour scale). Each value of the membrane potential corresponds to a value of the extracellular pH shown in Fig. 1D. The grey area indicates the PMF in the respirative regime; the pink area indicates the fermentative regime.

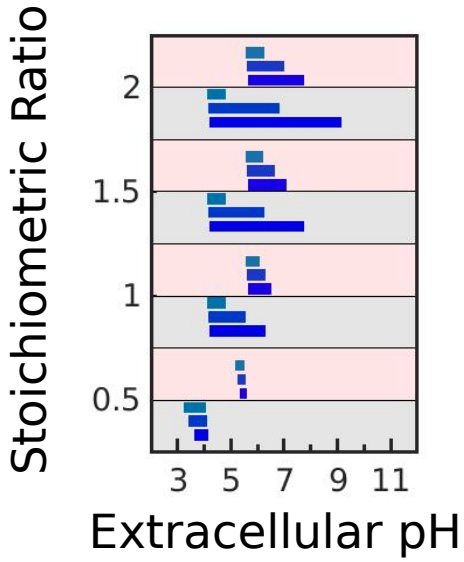

Fig. S6. Altering $z_Y[Y]_i$ and the PMF changes the range of extracellular pH over which *E. coli* is able to maintain a neutral pH$_i$. Following the approach of Fig. 1D, we show the predicted pH$_e$ ranges for two values of the PMF: -170 mV for the respirative regime in grey and -85 mV for the fermentative regime in pink. Each of the four antiporters of Fig. 1C are indicated by their stoichiometric ratio. We consider three different values of $z_Y[Y]_i$: -10 mM, 0, and +10 mM, shown using deep to light blue.

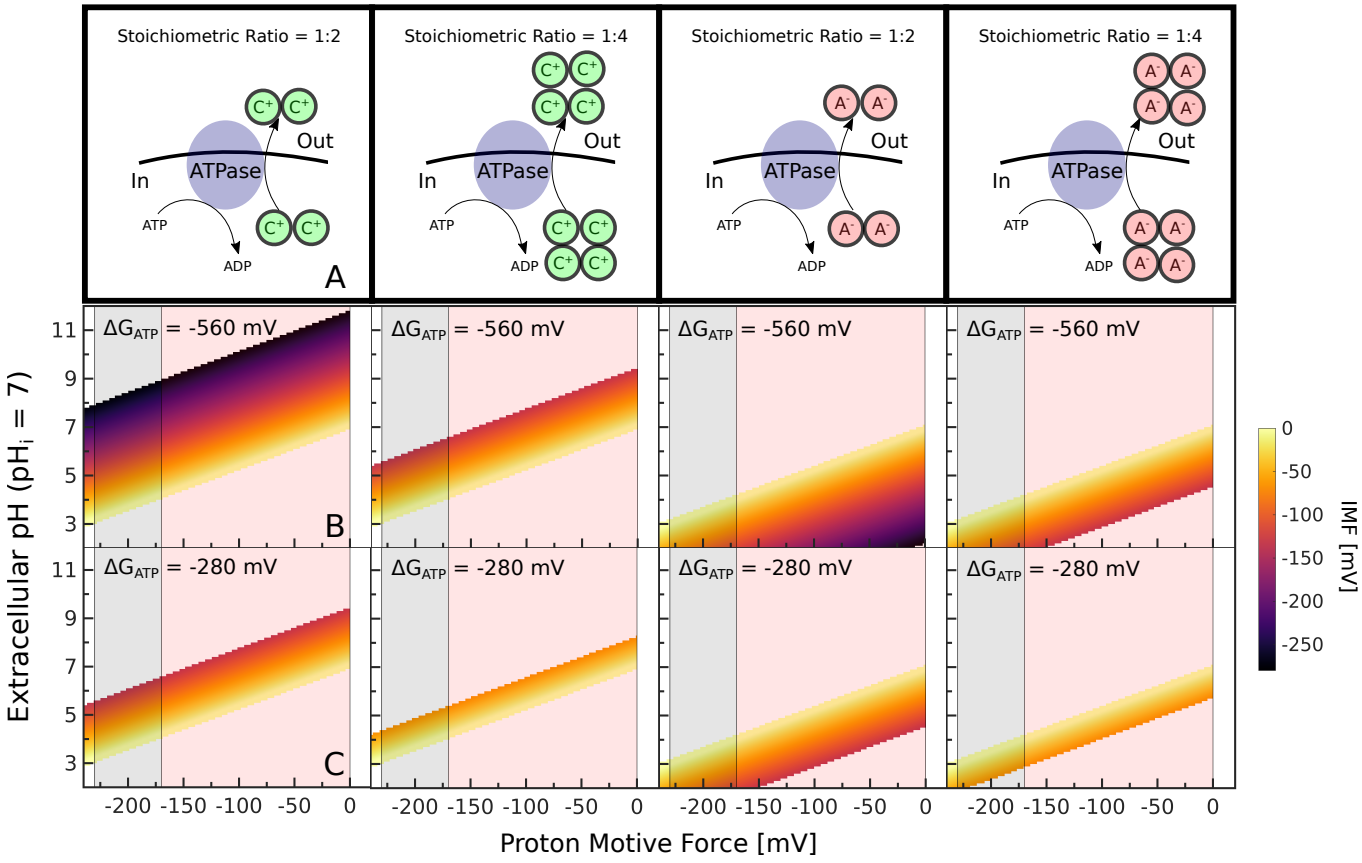

Fig. S7. The pH_e range over which cells can maintain a neutral pH_i does not scale with PMF if ATP-driven efflux pumps are used for generating physiological membrane potential. (A) Schematics of hypothetical ATP-driven ion efflux pumps we consider. (B) and (C) We plot the possible steady-state solutions for the hypothetical pumps for a given PMF between -240 and 0 mV, a pH_i of 7, and pH_e between 2 and 12. The average valency of captive molecules is bound between -1 and +1, osmotic pressure is set to 1 atm, and extracellular $[CA]_0$ = 100 mM. Grey and red shading shows values of the PMF expected for respiration and fermentation. The colour scale indicates the ionic motive force (IMF). (B) shows the case where the free energy of ATP hydorlysis is -560 mV and (C) -280 mV. Halving ΔG_{ATP} is equivalent to halving the stoichiometric ratio of the ATP efflux pump. Contrary to the case when ion efflux is powered by the PMF, i.e. is a consequence of the action of proton-ion antiporters, the range of pH_e at which pH_i can be maintained does not scale with the PMF. Both ways of powering ion efflux however result in loss of pH_i homeostasis at acidic pH_e upon loss of PMF and when the cell pumps anions, and the ability to maintain pHi upon loss of PMF is impaired more when efflux is powered by PMF.

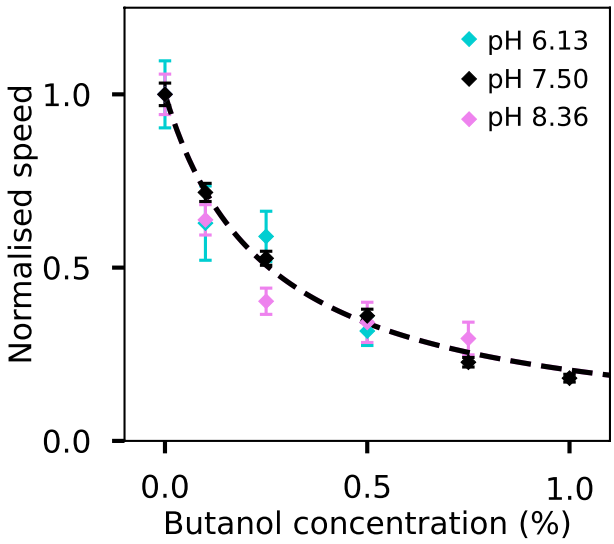

Fig. S8. The bacterial flagellar motor speed remains proportional to PMF within pH$_i$ 6.1 to 8.4 range. Bacterial flagellar motor speed has been found proportional to the PMF at different loads [40, 41]. Here we confirm that (at our chosen motor load) the motor speed remains proportional to PMF at different pH$_i$. For this purpose, *E. coli* cells were grown and prepared as described in the main text *Methods* section. To control pH$_i$ cells in our tunnel slide were exposed to the motility buffer (BMB, see *Methods* in the main text) of pH 6.13 or 8.36 containing 40 mM potassium benzoate and 40 mM methylamine hydrochloride, which equilibrates internal and external pH [42]. Next, we exposed the cells with pH$_i$ 6.13 and 8.36 to different butanol concentrations, where we know how the motor speed responds to different butanol concentrations at near neutral pH$_i$ from our previous studies [43]. The results are plotted together; previous results are in black, pink are the results for pH$_i$=6.13 and cyan 8.36. The black line shows a hyperbola fit also taken from [43] and the error bars show the standard error of the mean. Normalised speeds from different cells are plotted against the butanol concentration for each pH$_i$ (total of 24 cells for pH$_i$ 6.13 and 40 for 8.36). Normalised motor speeds follow the same trendline irrespective of pH$_i$.

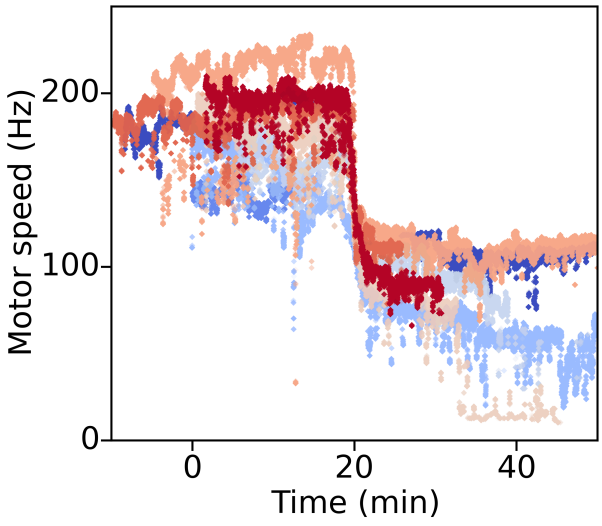

Fig. S9. In the absence of oxygen, the measured PMF approximately halves. Single-motor traces of *E. coli* cells (eight plotted using a different colour) in the sealed tunnel-slides at pH$_e$=7.0 in the presence of glucose. Cells are grown and prepared as described in the main text *Methods* section. Briefly upon harvesting cells are washed into BMB pH 7.0, supplemented with 20 mM glucose, and attached to the tunnel slide. Fresh BMB is flushed through the tunnel shortly before the recording, upon which the tunnel is sealed with a CoverGrip™ Coverslip Sealant to prevent oxygen exchange. The recording continues for 30-50 min. The traces are aligned by the time at which the motor speed drops – here shown at 20 min. The actual time point varied between 20 and 30 min depending on the concentration of cells and the period between sealing the tunnel-slide and beginning the recording. Speed drop indicates oxygen depletion in the medium, as reported in [44]

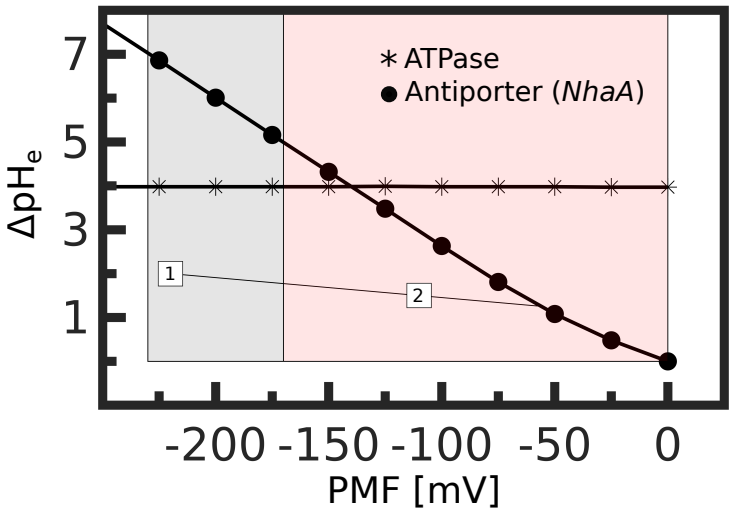

Fig. S10. pH$_e$ range over which the cells maintain near neutral pH$_i$ depends on the PMF value only if antiporters are responsible for generating $\Delta\psi$. pH$_e$ range over which cells maintain pH$_i$=7 is plotted for NhaA-line antiporter and for a putative ATP drive ion export pump. Only for the antiporter the pH$_e$ range depends on the value of the PMF. The two experimental data points, obtained for higher and lower absolute values of the PMF, are indicated in squares and are in agreement with the behaviour predicted for the antiporters (being responsible for the generation of $\Delta\psi$).

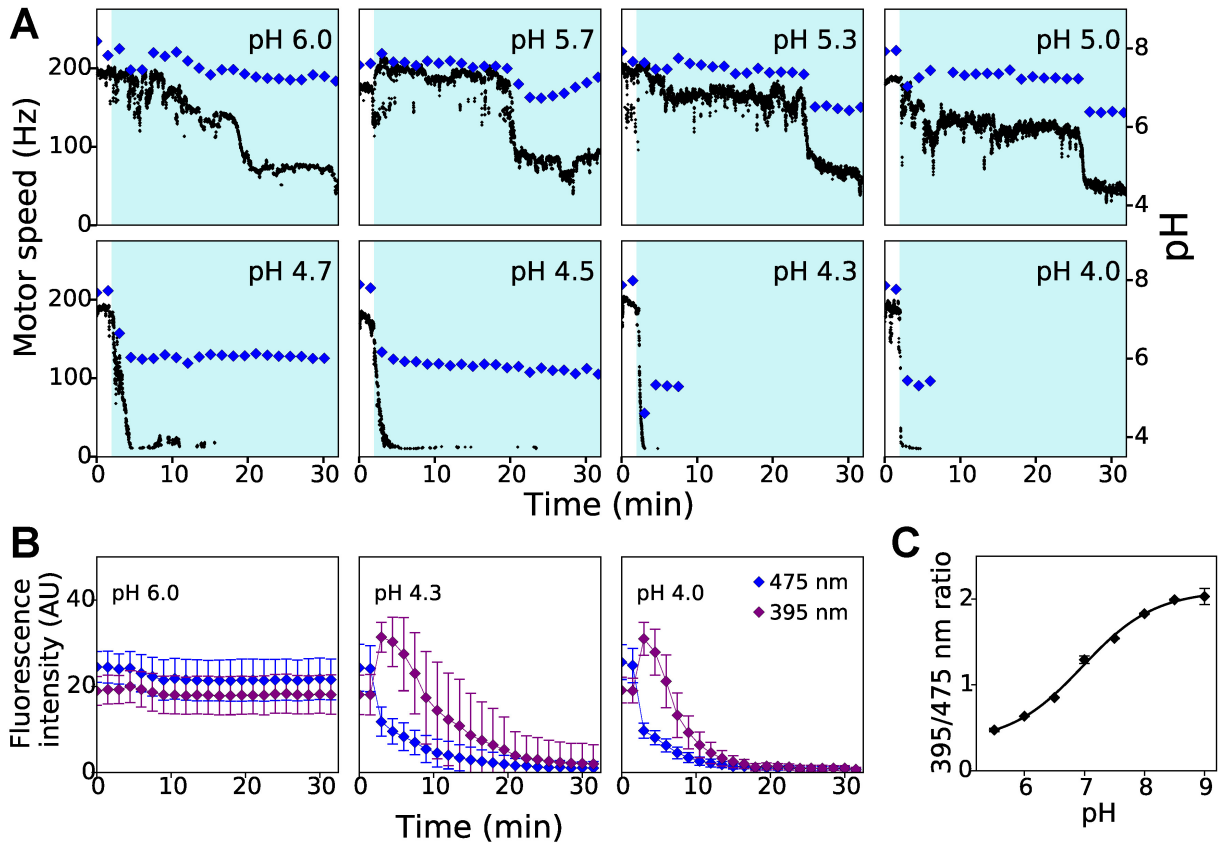

Fig. S11. Cells maintain neutral pH_i at $pH_e \geq 5.0$ for high magnitude PMF (i.e. in the presence of oxygen), and only at $pH_e \geq 5.5$ for lower PMF (in anaerobic conditions). (A) Single-cell examples of speed (in black) and pH_i (in blue) dynamics at different pH_e. Cells are prepared as described in the main text *Methods* section. At time t=0 to 2 min cells are in BMB, supplemented with 20 mM glucose at pH_e=7 (white background); at time point t=2 min low pH buffers are introduced (cyan region) and the slide is sealed. The sharp drop in motor speed observed in each example trace indicates the transition from aerobic to anaerobic metabolism, which happens 20-30 minutes after sealing the slide as shown also in S9 and in [44]. As the speed drops, pH_i drops as well. For $pH_e \geq 5.5$, pH_i recovers to neutral even after PMF loss, however, for $5.0 \leq pH_e \leq 5.5$ pH_i is maintained neutral only at higher motor speeds (i.e. in aerobic conditions) but not after oxygen is depleted. (B) pHluorin is not a suitable sensor for low pH_i because fluorescence is lost at low pH_e at both the relevant wavelengths of 475 nm and 395 nm. For each wavelength, we plot the averaged relative fluorescence intensity of $\approx$ 30 cells, grown and prepared for imaging as described in the main text *Methods* section (that also contains the imaging conditions). Error bars are the standard deviation of the pixels' intensities. (C) The sensitivity range of pHluorin spans pH 6–8.5. The calibration curve is reproduced from [45], where the pH gradient between the medium and the cytoplasm is collapsed by addition of 40 mM potassium benzoate and 40 mM methylamine hydrochloride and the buffers of known pH are used to calibrate pHluorin spectrum changes (see also *Methods* section in the main text). The mean 395/475 intensity ratio is plotted with the standard deviation against pH and fitted with a sigmoid function. Any pH_i lower than 5.5 will be detected as pH_i=5.5.

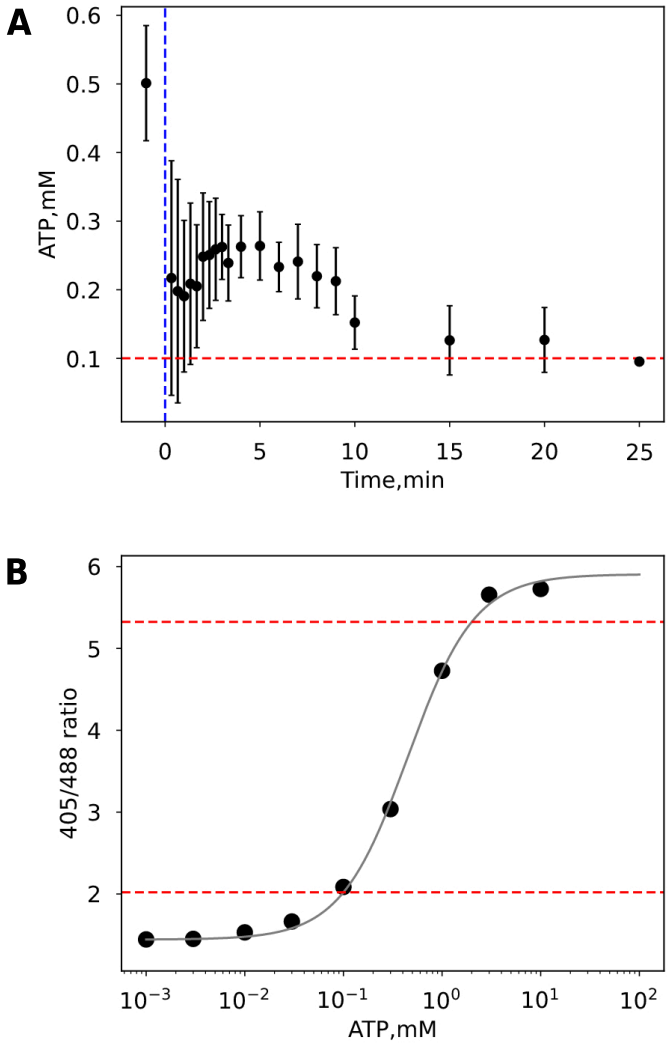

Fig. S12. *E. coli* maintain non-zero ATP levels for ∼10 min after the addition of 100 μM CCCP. (A) ATP concentration in *E. coli* cells measured with a fluorescent ratiometric Queen7μM* sensor [38], a modified version of Queen7μM [39]. Cells, carrying pWR-Q7* plasmid [38] are grown and prepared in BMB buffer with 20 mM glucose and pH 8.13 to 8.2 as described in the main text *Methods*. Fluorescence intensity is measured in the plate reader as described in the main text *Methods* with excitation at 405 and 488 nm and emission at 528 nm, and converted to [ATP] using the calibration curve in (B). A point is measured before CCCP addition. At time 0 (blue dashed line), 100 μM CCCP is added to the cells. The red dashed line shows the sensitivity limit of the Queen7μM* sensor, and error bars show the standard deviation of the mean between 4 replicates. (B) The calibration curve for Queen7μM* is obtained as in [38] using lysates of Queen7μM*-expressing cells and known ATP concentrations (see main text *Methods* section). The sensitivity range of the sensor spans from ∼0.1 to ∼2 mM ATP (red dashed lines).

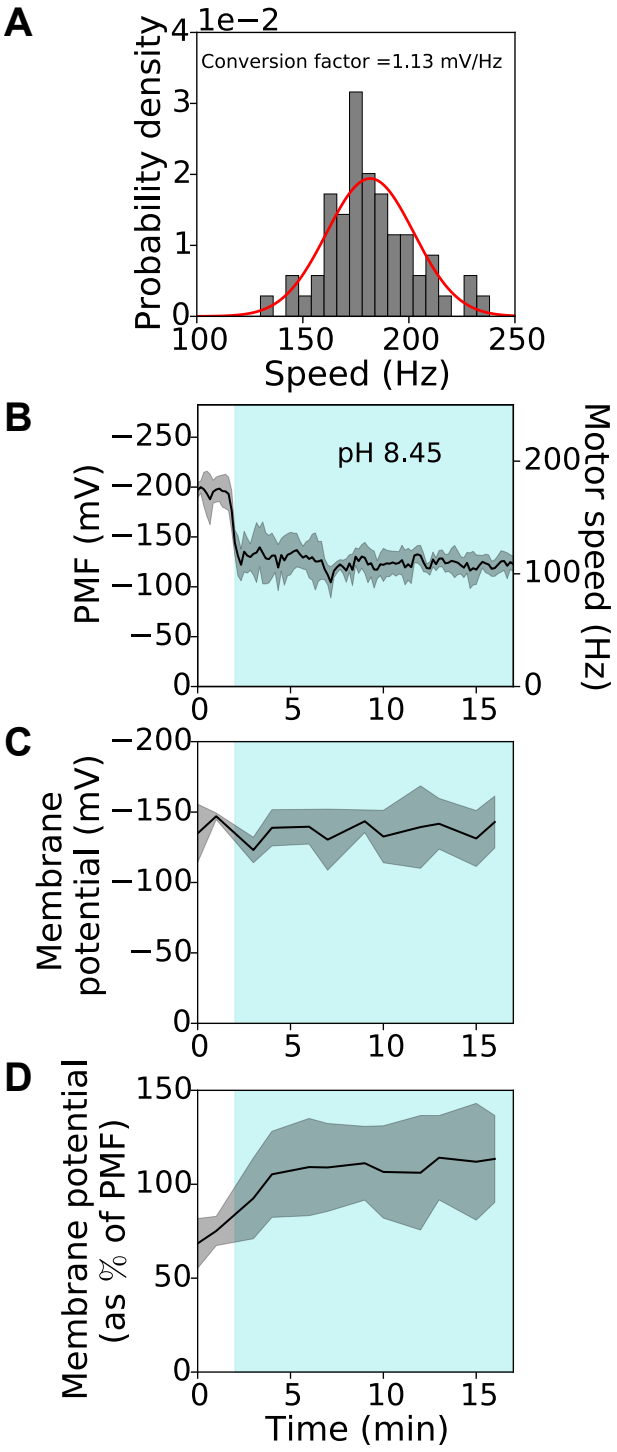

Fig. S13. Calibration of the PMF measured from the bacterial flagellar motor speeds. (A) The motor speed in BMB (see *Methods* in the main text) at pH_e=7.0 and in the presence of 20 mM glucose is converted to PMF using the predicted PMF range for cells respiring on glucose: $170 \leq |\text{PMF}| \leq 229$ mV. We combine 60 single-cell (single-motor) traces collected at pH_e = 7 and computed from 90 s long recordings. Cells were grown and prepared for tunnel slide recording as described in *Methods* section of the main text. The histogram of the resulting motor speeds is plotted – its median is 180.6 Hz; the red line shows a fit to a Gaussian distribution. We calculate the conversion factor that maximises the amount of traces within the predicted PMF range as $(170 + 229)/2/180.6 \approx 1.1$ mV/Hz. (B) The mean PMF of four cells, grown and prepared for imaging as described in the main text *Methods* section, experiencing an alkaline shift. Cell are kept in BMB (*Methods* in main text) with 20 mM glucose and pH_e=7 before the shift (white region), and pH_e=8.45 after the shift (cyan region). The PMF is calculated from the time series of motor speeds using the conversion factor from A. (C) The membrane potential and (D) the membrane potential relative to the PMF for the same data. The membrane potential is calculated from Eq. 3, where ΔG_{H+} is the PMF taken from B and the proton concentrations are found by measuring pH_i and pH_e. Errors are standard deviations.

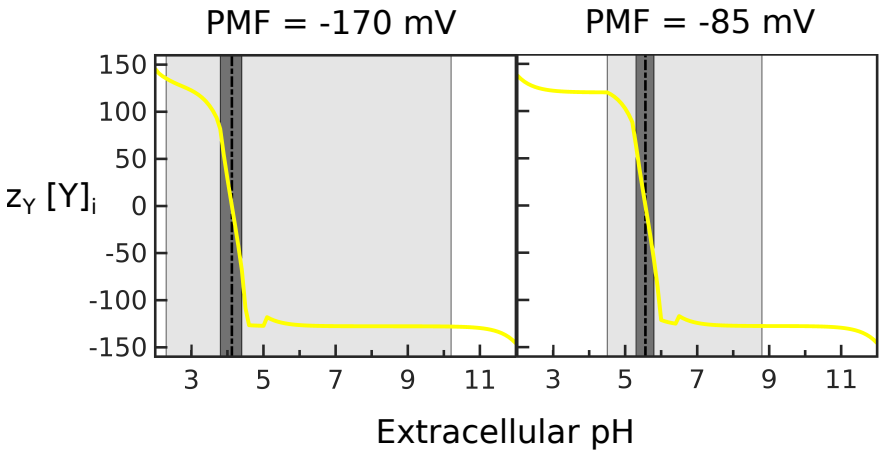

Fig. S14. The optimal valency changes sign as the pH$_e$ changes The numerical experiment is identical to that of Fig. 4 in the main text. We maintain pH$_i$ as closed as possible to 7, $-10 \leq z_Y \leq +10$, set the osmotic pressure to 1 atm and $[CA]_0$ to 50 mM. The black dotted line marks the pH$_e$ for which $\Delta\psi = 0$; to the left $\Delta\psi > 0$; to the right $\Delta\psi < 0$. The dark grey area indicates where the optimal solution has $\Delta G_{C^+} = \Delta G_{A^-} = 0$. The light grey area indicates where pH$_i$ can be maintained exactly at 7. For two different PMF values we show $z_Y\,[Y]_i$ that minimizes the cost of maintaining a steady-state (Eq. 15 in the main text).

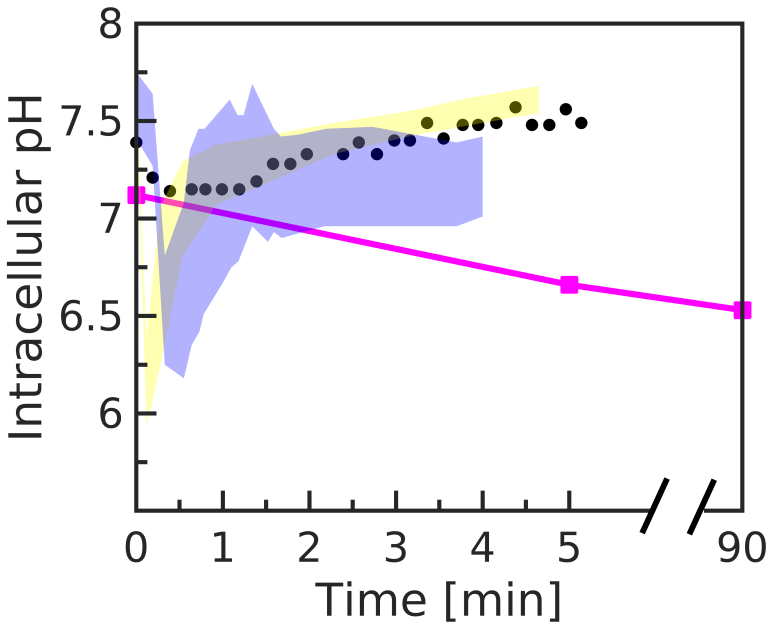

Fig. S15. Comparison of previous results on pH homeostasis We reproduce contradictory experimental results on the response of pH$_i$ in *E. coli* to changes in pH$_e$. Pink squares are for a pH$_e$ shift from 7.2 to 5.6 [46]. Black dots are population averages for a pH$_e$ shifted from 7.5 to 5.5 [47], and the yellow [48] and blue [42] shaded areas show the range of pH$_i$ measured in single cells for the same shift in pH$_e$.

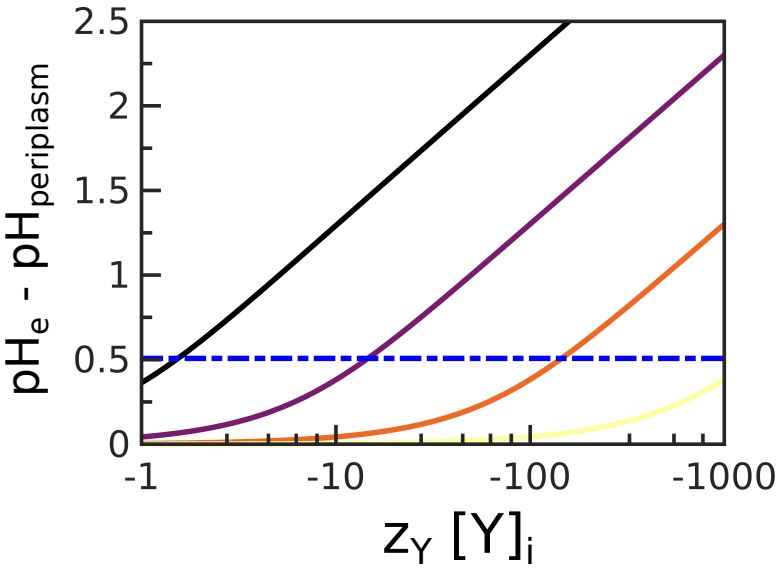

Fig. S16. The periplasmic membrane potential can offset the pH$_e$ 'felt' by the inner membrane. The difference between pH$_e$ and the periplasmic pH is plotted as a function of the periplasmic captive charges, $z_Y[Y]_p$, and for different values of [CA]$_0$: black to yellow show 1, 10, 100, and 1000 mM. Using the measured periplasmic radius, *E. coli*'s' periplasmic volume was estimated to be between 8 and 16% of the total cell volume [49] – we assume a value of 10%, and here do not consider osmotic pressure. In addition, we set pH$_e$=7 and let the periplasm be in ionic equilibrium with the environment. At low salinity (black and purple lines), the periplasmic captive charges offset the pH$_e$ 'observed' by the inner membrane. The difference between pH$_e$ at the inner membrane decreases with [CA]$_0$ even with little periplasmic captive charges.

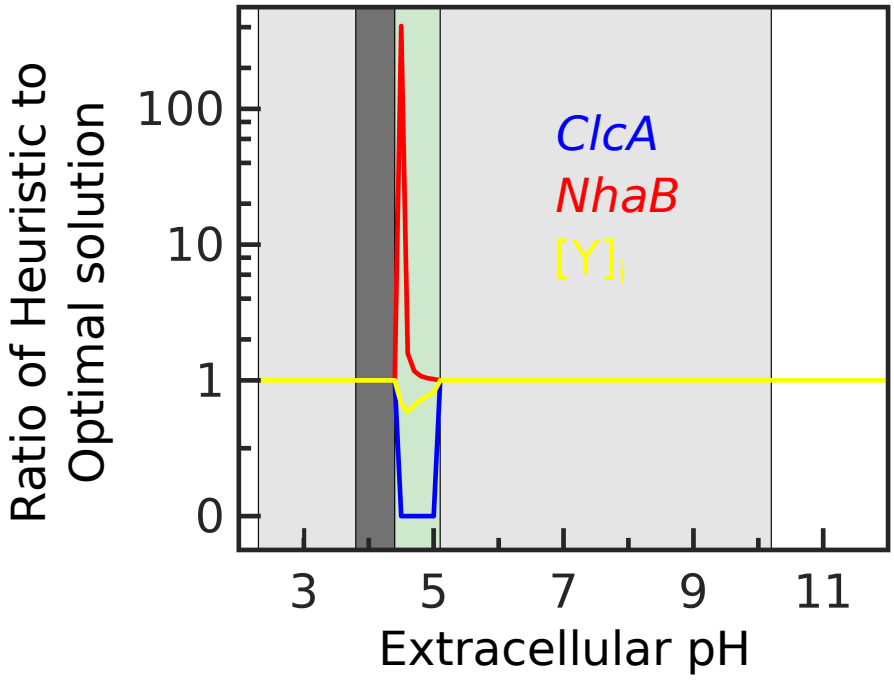

Fig. S17. Heuristic approximation for calculating cost in Eq. S52 gives very similar results to the optimal solution, that minimizes the cost. Both solutions set osmotic pressure to 1 atm, PMF to -170 mV and maintain pH$_i$ as close as possible to 7 (and exactly 7 in the light gray shaded area). Both solutions have identical average valency z_Y and intracellular concentration $[Y]_i$, as well as forward fluxes of all antiporters apart in the shaded green area. While the heuristic solution does not allow more than one antiporter to have non zero forward fluxe, the solution minimizing the cost has in this small pH$_e$ range positive forward fluxes for both *ClcA* and *NhaB* and smaller intracellular concentration of captive charges. In this pH$_e$ range the cost of powering antiporters is low (Main text figure 4) and the cell has less incentive to minimize the cost. The average valency of captive charges and forward flux for *NhaA* are identical for all pH$_e$ for the heuristic and optimal solutions.

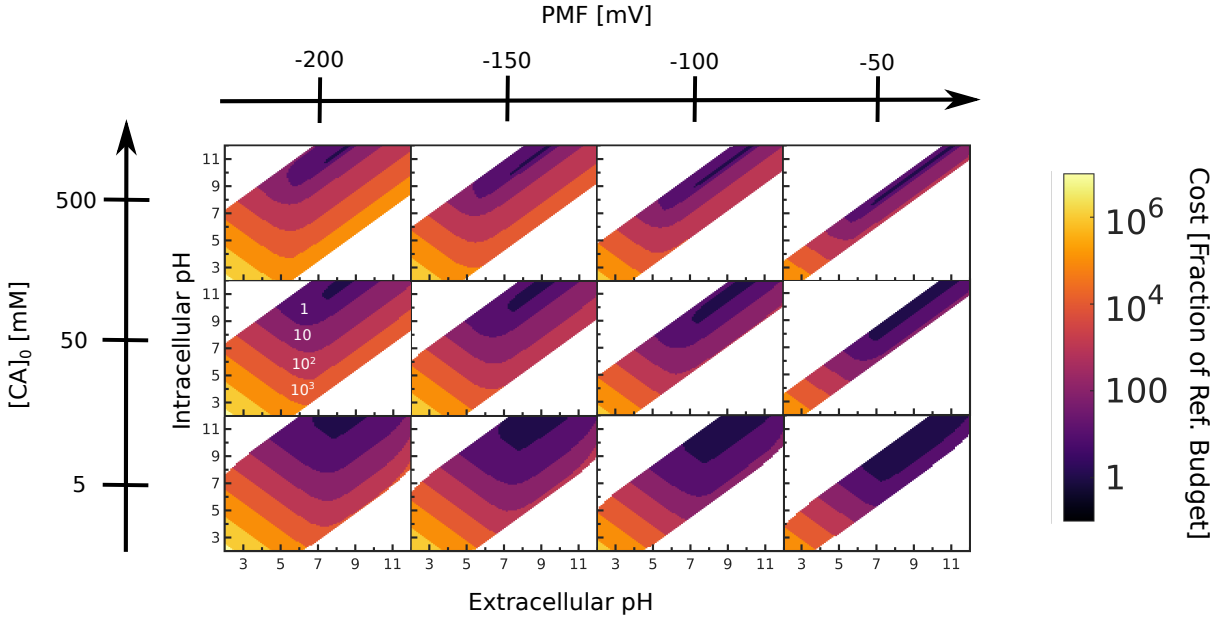

Fig. S18. The minimal cost of maintaining particular pH$_i$ and PMF for particular extracellular environments, determined by pH$_e$ and [CA]$_0$. We set the osmotic pressure to 1 atm and keep the average valency $-10 \leq z_Y \leq +10$, and calculate the minimal cost for a wider range of PMF values and [CA]$_0$. The cost is here estimated using the approximation for the optimal strategy calculation described above. White regions indicate PMF and pH$_i$ values that cannot be attained. White numbers give the cost value (corresponding to the colour scale).

References

1. Renata Buda, Yunxiao Liu, Jin Yang, Smitha Hegde, Keiran Stevenson, Fan Bai, and Teuta Pilizota. Dynamics of Escherichia coli s passive response to a sudden decrease in external osmolarity. Proc. Natl. Acad. Sci. USA, 113(40):E5838–E5846, oct 2016.

2. Markus Basan, Manlu Zhu, Xiongfeng Dai, Mya Warren, Daniel Sévin, Yi-Ping Wang, and Terence Hwa. Inflating bacterial cells by increased protein synthesis. Mol Syst Biol, 11(10):836, 2015.

3. Sattar Taheri-Araghi, Serena Bradde, John T. Sauls, Norbert S. Hill, Petra Anne Levin, Johan Paulsson, Massimo Vergassola, and Suckjoon Jun. Cell-size control and homeostasis in bacteria. Current Biology, 25(3):385–391, 2015.

4. Daniel A. Beard and Hong Qian. Chemical Biophysics: Quantitative Analysis of Cellular Systems. Cambridge Texts in Biomedical Engineering. Cambridge University Press, 2008.

5. Matteo Polettini and Massimiliano Esposito. Irreversible thermodynamics of open chemical networks. I. Emergent cycles and broken conservation laws. J Chem Phys, 141(2):024117, 2014.

6. J. Keener and J. Sneyd. Mathematical Physiology: I. Springer, New York, New York, 2009.

7. Keith D. Garlid, Andrew D. Beavis, and Signe K. Ratkje. On the nature of ion leaks in energy-transducing membranes. Biochim Biophy Acta, 976(2):109 – 120, 1989.

8. K. A. Dill and S. Bromberg. Molecular driving forces. Garland, New York, New York, 2011.

9. DC Tosteson and JF Hoffman. Regulation of cell volume by active cation transport in high and low potassium sheep red cells. J Gen Physiol., September 1960.

10. Alan R. Kay. How cells can control their size by pumping ions. Frontiers in Cell and Developmental Biology, 5, 2017.

11. Kira M Düsterwald, Christopher B Currin, Burman Richard J, Colin J Akerman, Alan R Kay, and Jospeh V Raimondo. Biophysical models reveal the relative importance of transporter proteins and impermeant anions in chloride homeostasis. eLife, September 2018.

12. Yi Deng, Mingzhai Sun, and Joshua W. Shaevitz. Direct measurement of cell wall stress stiffening and turgor pressure in live bacterial cells. Phys Rev Lett, 107:158101, Oct 2011.

13. Janet M. Wood. Bacterial responses to osmotic challenges. The Journal of general physiology, 145(5):381–388, May 2015. 25870209[pmid].

14. P. Mitchell. Coupling of phosphorylation to electron and hydrogen transfer by a chemi-osmotic type of mechanism. Nature, 191(4784):144–148, Jul 1961.

15. Bryson D Bennett, Elizabeth H Kimball, Melissa Gao, Robin Osterhout, Stephen J Van Dien, and Joshua D Rabinowitz. Absolute metabolite concentrations and implied enzyme active site occupancy in Escherichia coli. Nat Chem Biol, 5(8):593–599, 2009.

16. Stefan Steigmiller, Paola Turina, and Peter Gräber. The thermodynamic H^+/ATP ratios of the H^+-ATP synthases from chloroplasts and Escherichia coli. Proc Nat Acad Sci USA, 105(10):3745–3750, 2008.

17. Avi Flamholz, Elad Noor, Arren Bar-Even, and Ron Milo. eQuilibrator—the biochemical thermodynamics calculator. Nucleic Acids Res, 40(D1):D770–D775, 2012.

18. P.R. Rich. The molecular machinery of Keilin's respiratory chain. Biochemical Society Transactions, 31(6):1095–1105, 12 2003.

19. David B. Hicks, Jun Liu, Makoto Fujisawa, and Terry A. Krulwich. F1f0-atp synthases of alkaliphilic bacteria: Lessons from their adaptations. Biochimica et Biophysica Acta (BBA) - Bioenergetics, 1797(8):1362 – 1377, 2010.

20. Christoph von Ballmoos, Alexander Wiedenmann, and Peter Dimroth. Essentials for atp synthesis by f1f0 atp synthases. Annual Review of Biochemistry, 78(1):649–672, 2009. PMID: 19489730.

21. Guadalupe Guerra, Federico Martinez, and Juan Pablo Pardo. On the $H^+/2e^-$ stoichiometry of the respiratory chain. Biochem Mol Biol Educ, 30(6):363–367, 2002.

22. E Pinner, E Padan, and S Schuldiner. Kinetic properties of NhaB, a Na^+/H^+ antiporter from Escherichia coli. J Biol Chem, 269(42):26274–26279, 1994.

23. D Taglicht, E Padan, and S Schuldiner. Overproduction and purification of a functional Na^+/H^+ antiporter coded by nhaA (ant) from Escherichia coli. J Biol Chem, 266(17):11289–11294, 1991.

24. D Taglicht, E Padan, and S Schuldiner. Proton-sodium stoichiometry of NhaA, an electrogenic antiporter from Escherichia coli. J Biol Chem, 268(8):5382–7, 1993.

25. Alessio Accardi and Christopher Miller. Secondary active transport mediated by a prokaryotic homologue of ClC Cl^- channels. Nature, 427(6977):803–807, 2004.

26. Wei Bai, K.S. Zhao, and K. Asami. Dielectric properties of E. coli cell as simulated by the three-shell spheroidal model. Biophy Chem, 122(2):136 – 142, 2006.

27. K B Andersen and K von Meyenburg. Are growth rates of Escherichia coli in batch cultures limited by respiration? J Bacteriol, 144(1):114–123, 1980.

28. H Bremer and Patrick P Dennis. Modulation of chemical composition and other parameters of the cell by growth rate. Escherichia coli and Salmonella: cellular and molecular biology, 2(2):1553–69, 1996.

29. Terry J. Beveridge. Structures of Gram-negative cell walls and their derived membrane vesicles. J Bacteriol, 181(16):4725–4733, 1999.

30. Daniel O. Daley, Mikaela Rapp, Erik Granseth, Karin Melén, David Drew, and Gunnar von Heijne. Global topology analysis of the Escherichia coli inner membrane proteome. Science, 308(5726):1321–1323, 2005.

31. The UniProt Consortium. UniProt: a worldwide hub of protein knowledge. Nucleic Acids Res, 47(D1):D506–D515, 11 2018.

32. H. Nikaido. Molecular basis of bacterial outer membrane permeability revisited. Microbiol Mol Biol Rev, 2003.

33. Wonpil Im and Benoit Roux. Ion permeation and selectivity of OmpF porin: a theoretical study based on molecular dynamics, Brownian dynamics, and continuum electrodiffusion theory. J Mol Biol, 322(4):851 – 869, 2002.

34. J B Stock, B Rauch, and S Roseman. Periplasmic space in Salmonella typhimurium and Escherichia coli. J Biol Chem, 252(21):7850–61, 1977.

35. Renata Buda, Yunxiao Liu, Jin Yang, Smitha Hegde, Keiran Stevenson, Fan Bai, and Teuta Pilizota. Dynamics of Escherichia coli's passive response to a sudden decrease in external osmolarity. Proc Nat Acad Sci USA, 113(40):E5838–E5846, 2016.

36. P F Costa, M G Emilio, P L Fernandes, H G Ferreira, and K G Ferreira. Determination of ionic permeability coefficients of the plasma membrane of Xenopus laevis oocytes under voltage clamp. J Physiol, 413(1):199–211, 1989.

37. Robert J. Silbey, Robert A. Alberty, and Moungi G. Bawendi. Physical Chemistry. Wiley, 2004.

38. Leonardo Mancini and Teuta Pilizota. Environmental conditions define the energetics of bacterial dormancy and its antibiotic susceptibility. Biophysical Journal, 122(16):3207–3218, 2023.

39. Hideyuki Yaginuma, Shinnosuke Kawai, Kazuhito V. Tabata, Keisuke Tomiyama, Akira Kakizuka, Tamiki Komatsuzaki, Hiroyuki Noji, and Hiromi Imamura. Diversity in ATP concentrations in a single bacterial cell population revealed by quantitative single-cell imaging. Scientific Reports, 4(1):6522, October 2014.

40. David C. Fung and Howard C. Berg. Powering the flagellar motor of Escherichia coli with an external voltage source. Nature, 375(6534):809–812, 1995.

41. Christopher V Gabel and Howard C Berg. The speed of the flagellar rotary motor of Escherichia coli varies linearly with protonmotive force. Proc. Natl. Acad. Sci. U. S. A., 100(15):8748–8751, jul 2003.

42. Keith A. Martinez, Ryan D. Kitko, J. Patrick Mershon, Haley E. Adcox, Kotiba A. Malek, Melanie B. Berkmen, and Joan L. Slonczewski. Cytoplasmic ph response to acid stress in individual cells of escherichia coli and bacillus subtilis observed by fluorescence ratio imaging microscopy. Applied and Environmental Microbiology, 78(10):3706–3714, 2012.

289 43. Ekaterina Krasnopeeva, Chien-Jung Lo, and Teuta Pilizota. Single-cell bacterial electrophysiology reveals mechanisms of
290 stress-induced damage. Biophysical Journal, 116(12):2390 – 2399, 2019.

291 44. Jana Schwarz-Linek, Jochen Arlt, Alys Jepson, Angela Dawson, Teun Vissers, Dario Miroli, Teuta Pilizota, Vincent A.
292 Martinez, and Wilson C.K. Poon. Escherichia coli as a model active colloid: A practical introduction. Colloids and
293 Surfaces B: Biointerfaces, 137:2–16, jan 2016.

294 45. Yao Kuan Wang, Ekaterina Krasnopeeva, Ssu-Yuan Lin, Fan Bai, Teuta Pilizota, and Chien-Jung Lo. Comparison of
295 Escherichia coli surface attachment methods for single-cell microscopy. Sci Rep, 9:2019, 2019.

296 46. Smarajit Chakraborty, Ricksen S. Winardhi, Leslie K. Morgan, Jie Yan, and Linda J. Kenney. Non-canonical activation of
297 ompr drives acid and osmotic stress responses in single bacterial cells. Nature Communications, 8(1):1587, 2017.

298 47. Joan L. Slonczewski, Robert M. Macnab, Jeffry R. Alger, and Anna M. Castle. Effects of ph and repellent tactic stimuli
299 on protein methylation levels in escherichia coli. Journal of Bacteriology, 152(1):384–399, 1982.

300 48. Jessica C. Wilks and Joan L. Slonczewski. ph of the cytoplasm and periplasm of escherichia coli: Rapid measurement by
301 green fluorescent protein fluorimetry. Journal of Bacteriology, 189(15):5601–5607, 2007.

302 49. B. Oliver Donald and F. C. Neidhardt. Escherichia coli and Salmonella: Cellular and Molecular Biology. Volume 1. ASM
303 Press, 1996.